공학박사 학위논문

# Reactive Polymer Platforms Based on Atom Transfer Radical Polymerization of Pentafluorophenyl Methacrylate and Their Applications

팬타플로오로페닐 메타크릴레이트의 원자전이 라디칼 중합을 기반으로 한 반응성 고분자 플랫폼 제조 및 응용에 관한 연구

**2016 년 2 월**

서울대학교 대학원

화학생물공학부

이 연 주

# Abstract

During the past decades, functional polymers have been emerging as a promising candidate for advanced materials in a wide range of application fields such as biotechnology, photonics, and optoelectronics with advanced properties such as fluorescence, stimuli-responsiveness, and biocompatibility. Depending on particular application, the properties and nanostructures of functional polymer should be tailed to achieve those of interested. As requirements on functional polymers become more complicated, tedious synthesis and polymerization were often required to realize polymers with desired functionalities and structures. Furthermore, modification of pre-formed structure is difficult and extensive. Thus, modular platforms that allow facile synthesis and modification are highly desired.

Activated ester containing monomers have been extensively studied to demonstrate modular synthesis of versatile functional polymers by simple modification with various amine. More specifically, pentafluorophenyl methacrylate (PFPMA) has been actively studied since it has high reactivity with various amines, better controllability, and stability than *N*-hydroxysuccinimide (NHS) and their acrylate counterpart. While reversible addition-fragmentation chain-transfer (RAFT) of PFPMA has been intensively reported, reports on the atom transfer radical polymerization (ATRP) of PFPMA are rare due to poisoning

of catalyst and initiator by reacting monomer with them.

ATRP is one of valuable tool to design and synthesis of polymer with various composition and topology. Furthermore, various components for ATRP allow fine control of growing radical, resulting pre-determined molecular weight and narrow polydispersity index. All components for ATRP are also free from difficult synthesis step since most of chemicals are commercially available. The cumbersome optimization of ATRP condition for new functional monomers is one of challenges for wide application of ATRP. By combining merits of PFPMA with ATRP, this challenge enable to be solve. Optimized condition with proper components is obtained after series of ATRP of PFPMA under various condition. Details about kinetics studies on ATRP of PFPMA will be discussed in chapter 2.

With optimized conditions for controlled ATRP of PFPMA in hand, we demonstrate reactive polymer nanoparticle (PNP) platforms, which enable to convert their functionalities, by nanoprecipitation that allows fast and simple preparation of nanoparticles without surfactant (chapter 3). Fluorescent polymer nanoparticles are realized by simple modification of reactive polymer with commercially available dansylcadaverine as a model study. Control of size, size distribution and photophysical properties are studied. Well-defined fluorescent nanoparticles are prepared and those show 4.5 fold enhanced relative quantum yields compared with dansylcadaverine in water. Our strategy allows facile and modular synthesis of functional polymer nanoparticles with desired properties. Furthermore, imparting other functions on nanoparticles are enabled by further

modification of remaining activated ester group. Structural stability, however, should be ensured during further modification to prevent dissolution of polymer in various organic solvent.

By employing coumarin that enable to undergo photo-reversible dimerization into reactive polymer, robust, reactive PNP platforms have been realized. Using light as an external trigger for cross-link, structural stability enable to be obtained without destruction of structure and inter-particle cross-link. Reactive PNP platforms are treated with not only small molecules including isopropylamine, *N*-(2-aminoehtyl)-3-(3',3'-dimethyl-6-nitrospiro[chromene-2,2'-indolin]-1'yl) propanamide (spiro-pyran-amine), or dansylcadaverine, but also amine terminated polymer (poly(*N*-isopropylacrylamide) (poly(NIPAAm)) to prove the possibility of further modification. Through DLS and photo physical studies, we confirm that resulting functional PNPs show thermo-, and photo-responsiveness, respectively.

In chapter 4, reactive polymer brushes platform is demonstrated by surface-initiated (SI)-ATRP of PFPMA from ITO surface for electrical application. Polymerization of PFPMA is conducted with ITO modified by immersing into different concentration of initiator solution in toluene. AFM measurement confirms that height of optimized poly(PFPMA) on ITO (ITO-g-p(PFPMA)) is 8 nm and grafting density of that is 0.2 chains/$mn^2$. The reactive polymer brush platform is treated with 4-amino-2,2,6,6,-tetramethylpiperidine 1-oxyl (4-amino-TEMPO) which has bistable state (or called as redox properties) to impart electrochemical properties on surface. Surface characterization conducted with FT-IR and x-ray

photoelectron spectroscopy (XPS) confirm that the PFP group was successfully replaced to TEMPO molecules (yields =100 %, calculated by XPS).

In conclusion, modular platforms that allow facile and modular synthesis of functional material are demonstrated from monomer to polymer and polymer to nanostructures. We believe that our system and the strategy used for its achievement constitutes a novel approach that provides a facile process towards functional polymer, polymer nanoparticles, and polymer brushes and widening the application of polymer by eliminating difficult multistep of synthesis.

**Keyword :** Functional polymers, reactive polymers, atom-transfer radical polymerization, fluorescent polymer nanoparticles, stimuli-responsive polymer nanoparticles, reactive polymer brushes.

**Student Number :** 2009-23954

# Contents

# List of Figures

# List of Tables

# Chapter 1. Introduction

## 1.1. Definition and classification of functional polymers

Functional polymers are justified as polymers with advanced properties such as optic, electronic, and/or biocompatibility. The studies on functional polymers have been increased since these allow low cost production with facile processing in a wide range of applications such as biotechnology, photonics, and optoelectronics. Depending on the represent properties, these enable to classify as semiconducting conjugated polymers (fluorescent polymers), stimuli-responsive (smart) polymers, biomimetic materials, and metallopolymers.

Since first description on polyaniline was reported by Henry Lentheby[1] semiconducting conjugated polymers which shows electric conductivity have been intensively studied to understand the mechanism and enhance the conductivity. Alan J. Heeger, Alan Macdiamid and Hideki Shirakawa awarded the 2000 Nobel Prize in Chemistry “for the discovery and development of conductive polymer” based on their work reported in 1977.[2] One of promising properties of those polymers is electric conductive. By controlling monomer structure, highest occupied molecular orbital (HOMO) and lowest unoccupied molecular orbital (LUMO) level of polymer could be tuned. When the polymer gains energy from electricity or photon, electron of HOMO level jump into LUMO level and electron

become conductive through conjugated backbone or come back to LUMO level with light emission. Depending on difference between HOMO and LUMO, the emission wavelength of polymer is changed and emits different color. When polymer emit light by electric current, this behavior is called as electroluminescence.[3] Semiconducting polymers are also able to emit light by photon, and this behavior is called as a photoluminescence.[4] The polymer containing fluorescent pendant also enables to emit light while those are not or less electric conductive since electron can flow by jumping to the neighbor molecules. With those properties, semiconducting polymers can be applied to (opto) electronic such as organic solar cell,[5-8] and organic light emitting diode (OLED),[9], [10] imaging,[11], [12] and sensors[13], [14]

Stimuli-responsive (smart) polymers[15] are smart polymers that convert their properties or structures according to external triggers such as temperature,[16], [17] humidity, pH,[16] light,[18], [19] or electric or magnetic field.[20] More specifically, thermo-responsive polymers have lower critical solution temperature (LCST) or upper critical solution temperature (UCST) which are critical temperature point where polymer and solvent are completely miscible below or above, respectively. Thermo-responsive polymer like poly (*N*-isopropylacrylamide) (PNIPAM) was demonstrated as a nanogel, micelle, and polymer film.[17], [21], [22] Weak polyelectrolyte, which shows responsibility for pH, such as poly(acrylicacid) (PAA),[23] poly(methacrylicacid),[24] and poly(allylamine hydrochloride (PAH)[25] was used for sensor or durg delivery. Polymer containing photochromic dyes like

spiropyran show color change upon light irradiation and also wetterabiliy.[19] Since those polymer can change properties including conformation,[22] adhesiveness,[26] or water retention,[27] these materials are playing an increasingly important role in a wide range of application such as biotechnology,[25], [28] and smart optical system.[29]

Biomimetic materials are materials modeled after nature or that enable to easily realize structure inspired from nature. Polydopamine[30] which is inspired by the composition of adhesive proteins in mussels is representative for biomimetic materials. Polysaccharide[31] has been also intensively studied as a biomolecules. Unique structure from nature such as gecko`s feet[32] and lotus leaf[33] are also studied to understand mechanism. Mimicking the fly trap is also excellent example for preparing smart actuator which response from stimuli. Those materials are applied in biotechnology, adhesion, self-cleaning surface.

Since the 1990s, well-characterized high molecular weight metallopolymers[34] which are synthetic polymers containing metal centers reported for the first time, those metallopolymers[35] are emerging as a promising materials. With unique properties from metal center, those allows facile process of materials. A diverse range of different metal center including Fe,[36], [37] Ru, [38], [39] and Zn[40] has been studied to tune its properties such as electro-, photoluminescence,[38] supramolecular assemblies,[36] and electronic magnetic interactions.[39] With those properties, metallopolymers can be applied in LED, photovoltaics, and sensors.

Depending on their functionality, careful choice of synthetic and processing methods are required to prepare desired structure with functionality. In section 1.2,

we will focus on preparation methods of functional polymers.

## 1.2. Synthesis and processing of functional polymers

As requirements on polymers become more complicated and specific, various synthetic techniques and processing methods have been developed to satisfy demands for particular applications. The functional polymers enable to be prepared by polymerization of functional monomers[41], [42], [43] or post-polymerization modification through specific technique called as click chemistry[44] like thiol-ene reaction,[45] Diels-Alder Chemistry,[46] and Michael addition.[47] Development of polymerization technique including living radical polymerization (i.e., anionic polymerization), controlled radical polymerization (i.e., atom transfer radical polymerization (ATRP), reversible addition-fragmentation chain-transfer (RAFT), and nitroxide mediated polymerization (NMP)), ring-opening metathesis polymerization (ROMP) and step grow (i.e., Suzuki coupling reaction[48] under palladium catalyst, and condensation polymerization) allows fine control of chain growth and preparation of various function polymers. The details about post-polymerization modification of activated ester monomers will be discussed in section 1.3.

The structures of the functional polymers were tailored depending on the particular applications from aggregates to brushes. Those structures were enabled to classify into nanoparticles and films (Figure 1.1). The functional polymer nanoparticles, which are solid, or colloidal in the range from tens to thousands of nanometer, are enabled to be prepared either polymerization of functional

monomers by (mini)emulsion,[43] interfacial polymerization,[49] or living/controlled radical polymerization[50] or dispersion of polymer by solvent evaporation,[51] nanoprecipitation,[52] self-assembly[53] or supercritical fluid technology.[54] Depending on preparation methods, particles tend to have different morphology including aggregates, nanogel, hollow capsules, micelles, and colloids. Furthermore, inorganic precursors and particles were incorporated to enhance the properties of materials.

The functional polymer films including thin films, membranes, inorganic hybrid films, and brushes are also enabled to prepared by processing of polymers such as spin cast, drop cast, dip coating, layer-by-layer (LbL),[55] block copolymer assembly[56] or polymerization of monomer from the surface.[57], [58] Depending on required properties, specific technique should be chosen carefully. The modification of surface or interface with thin polymer films has been intensively studied for tuning surface properties such as wettability, biocompatibility, and corrosion resistance.

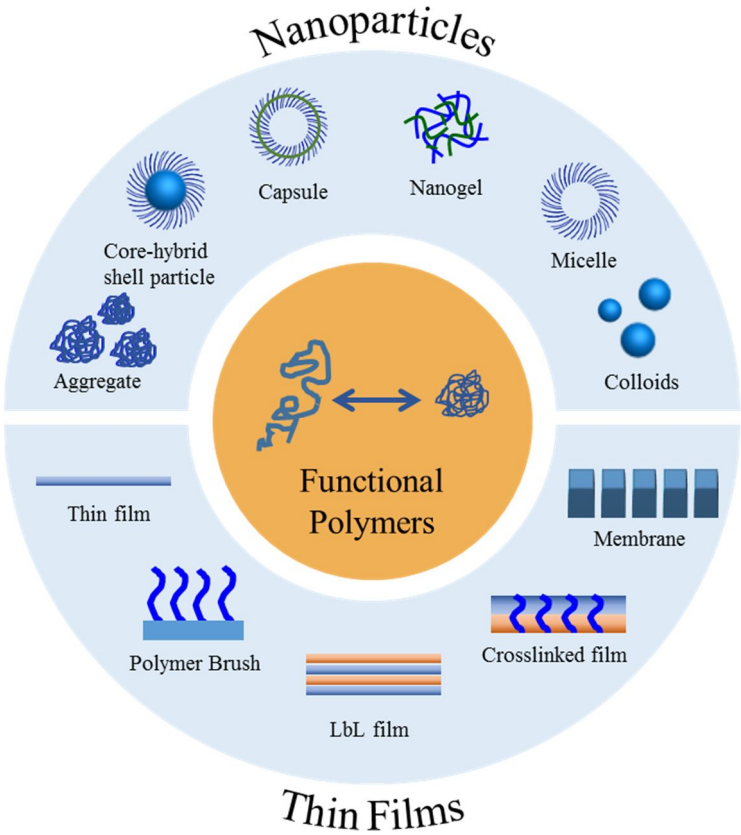


**Figure 1.1.** Illustration of classification for nanostructured functional polymer materials depending on structure (from nanoparticles to films). This illustration is redesigned from S. Sergiy Minko et. al.[15]

## 1.3. Activated ester monomers and polymers as scaffolds for functional polymers

As already discussed in previous section, giving functionalities on polymers is often required difficult design and synthesis of monomer structure, and cumbersome polymerization. Furthermore, direct polymerization of certain functional monomer often has limitation due to functional group tolerance under polymerization condition such as poisoning the initiator/catalyst or monomer or self-polymerization of functional group. Thus, studies on post polymerization modification have been intensively conducted. Most of earlier examples of post polymerization modification such as hydrogenation,[59] thiol-ene addition,[45] halogenation,[60] however, often has low quantitative conversion even under harsh reaction condition and potential for defects on polymer. In order to overcome efficiency of chemical reactions and reduce the possibility for side reaction, chemoselective-coupling reaction such as Michael addition,[47] nucleophilic activated cycloaddition,[61] Diels-Alder cycloaddition[46] and activated ester containing monomers were developed.

Since Ringsdorf[62] and Ferruti[63] introduced the concept of activated ester chemistry for preparing reactive polymers, many different kind of activated ester containing monomers such as *N*-hydroxysuccinimide (NHS) or aryl ester with electron withdrawing group were reported (Figure 1.2).[64] While NHS ester

containing monomers are the oldest and most popular one, poor solubility of their polymers in organic solvent (except DMF, DMSO) acts as major drawback. Among various aryl ester with electron withdrawing groups, pentafluorophenyl (PFP) ester-based monomers have been most intensively studied due to its less toxicity and steric hindrance compared to thrichlorophenyl and pentachlorophenyl ester-based monomer, respectively.[65] When synthesis of pentafluorophenyl acrylate (PFPA) and its polymer was first reported by Blazejewski and coworkers,[66] it has limitation on further characterization because of insolubility of the polymeric material. After Patrick and his co-worker reported synthesis of PFPA, pentafluorophenyl methacrylate (PFPMA), and their polymerization using AIBN, poly(PFPA) and poly(PFPMA) were enabled to soluble in wide range of organic solvent unlike poly(NHSA) or poly(NHSMA).[65] This advance allows not only characterization of polymers but also comparison of their reactivity with other type of activated ester containing monomers by treating them with primary, secondary, and aromatic amines as well as alcohols. In general, pentafluorophenyl (PFP) ester-based polymers show better reactivity than the NHS ester-based polymers. Among PFP ester based polymers, acrylate backbones were found to be slightly more reactive than methacrylate counterparts. After this advance, PFP ester-based polymers were polymerized under various living/controlled radical polymerizations such as ring-opening metathesis polymerization (ROMP),[67] reversible addition-fragmentation chain-transfer (RAFT) polymerization,[68] and nitroxide mediated radical polymerization (NMP),[69] while polymerization with atom transfer radical

polymerization (ATRP) is not efficient.

In this thesis, preparation of various functional polymer nanoparticles and polymer brushes will discussed by post polymerization modification of PFPMA polymerized by ATRP. In chapter 2, kinetics of ATRP with PFPMA will be discussed to optimize polymerization condition, which was acted as versatile scaffolds for realizing various structures. Demonstration of functional polymer nanoparticles was studied in chapter 3, by preparing reactive polymer nanoparticle platforms and modifying it with various functional molecules. In chapter 4, reactive polymer brushes were realized by surface initiated (SI-ATRP) from ITO for modified with electro active functional molecules to apply in electrical application fields.

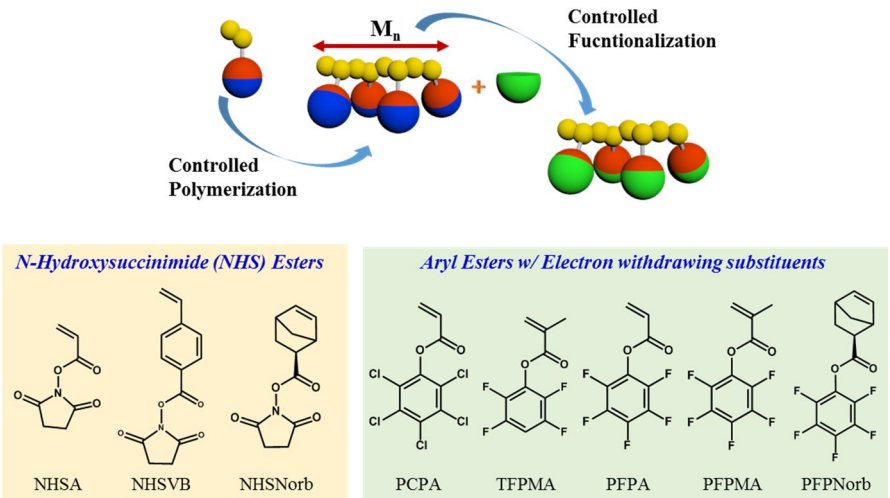


**Figure 1.2.** Schematic illustration for controlled radical polymerization and functionalities of activated ester containing monomers with example of *N*-hydroxysuccinimide (NHS) esters and aryl esters with electron withdrawing substituents. This illustration is redesigned from Theato.[64]

# Chapter 2. Polymerization of Pentafluorophenyl Methacrylate via Atom Transfer Radical Polymerization

## 2.1. Introduction

### 2.1.1. Atom transfer radical polymerization (ATRP)

ATRP is one of most promising techniques for preparing controlled molecular architecture with pre-determined molecular weight and narrow polydispersity index (PDI). By controlling dynamic equilibrium between propagating radicals and dormant species, ATRP allows fine control of composition (homo, block, alternating, gradient, and graft copolymers), chain topology (linear, stars, cycles, combs, regular networks, brushes), and diverse functionality.

When ATRP initiate from alkyl halides/macromolecular species ($P_nX$) by reacting with the rate constant of activation ($k_{act}$), the transition metal complexes change their oxidation state from lower state (activators), $Mt^m/L$ to higher state (deactivators), $Mt^{m+1}/L$, where $Mt^m$ is the transition metal in oxidation state m, and L is a ligand. Once the radical initiate, the growing radicals ($P_n$*) propagate with rate constant of propagation ($k_p$), and polymerize monomer. By reacting with

transition

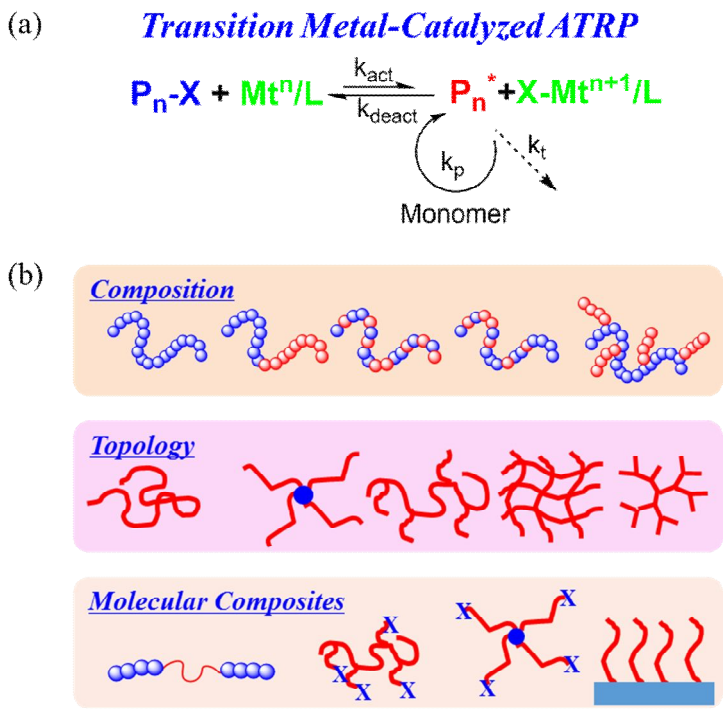


**Figure 2.1.** Illustration of (a) mechanism of transition metal-catalyzed ATRP and (b) possible examples of various compositions, topologies, and molecular composites.

metal complexes in higher oxidation state, growing radical ($P_n$*) deactivate in dormant species ($P_nX$) and the transition metal complexes change their oxidation state from higher state to lower state (Figure 2.1).[70]

The rate of an ATRP ($R_p$) depends on the rate constant of propagation ($k_p$) and on the concentration of monomer ([M]) and growing radicals ([$P_n$*]), which is related with equilibrium constant ($K_{ATRP}$), and the concentration of dormant species ([$P_nX$]), activators ([$Cu^I$/L]) and deactivators ([X-$Cu^{II}$/L]) (Equation 2.1). The dispersity of molecular weight of polymers prepared by ATRP under fast initiation without chain termination or transfer is determined by the concentration of dormant spices and deactivator, the rate constants of propagation and deactivation, and monomer conversion (p) (Equation 2.2). Those factors are strongly affected by choice of components as well as reaction conditions (solvent, temperature, pressure, ratio between components).[70-73]

$$R_P = k_p[M][P_n^*] = k_p K_{ATRP}\left(\frac{[P_nX][Cu^I/L][M]}{[X-Cu^{II}/L]}\right) \quad \textbf{Equation 2.1}$$

$$\frac{M_w}{M_n} = 1 + \frac{1}{DP_n} + \left(\frac{k_p[P_nX]}{k_{deact}[X-Cu^{II}/L]}\right)\left(\frac{2}{p}-1\right) \quad \textbf{Equation 2.2}$$

Components of ATRP consist of alkyl halide initiator, transition metal catalysts, monomers, and ligands. Depending on selected monomer, structure of initiator should be chosen carefully since initiation should be faster than

propagation for successful ATRP initiating system (Figure 2.2). The $k_{act}$ values of various initiator are different depending on their structure and kinds of halide. The $k_{act}$ values follow the order tertiary (3°) > secondary (2°) > primary (1°) alkyl halide ester initiator, and R-I > R-Br > R-Cl since chloride has more strong bond than iodide.[74] Furthermore, various redox-active transition metal complexes such as Cu, Ru, Fe, Mo, Os has been investigated. Copper, however, has been most often used since its accessibility.[70] Various monomers including commercial methyl acrylate (MA), (metha)acrylate ((M)A), and styrene as well as functional monomers enable to polymerize under ATRP system. Various ligands based on nitrogen have been used for ATRP and show different $k_{act}$ depending on number of nitrogen and structure, so $k_{act}$ is decreased with decreasing number of nitrogen and from aryl amine to pyridine.[72] Although those various factors and components allow fine control of molecular weight and PDI as well as molecular architecture for polymers prepared by ATRP, cumbersome and tedious optimization of ATRP condition for particular monomer of interest is often required.

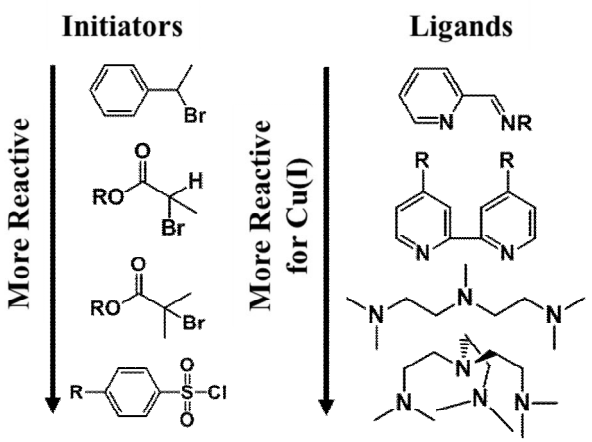


**Figure 2.2.** Tendency on reactivity of ATRP depending on structure of initiators and ligands.

## 2.1.2. Pentafluorophenyl methacrylate (PFPMA)

Combining merits of ATRP and PFPMA provide a solution for eliminating optimizing step for preparing new functional polymers. Once the ATRP condition for PFPMA was optimized, minutely controlled functional polymers enabled to be prepared by treating poly(pentafluorophenyl methacrylate) (poly(PFPMA)) with amine containing molecules with particular functions. While RAFT polymerization has been fully studied as already discussed in section 1.3, studies on ATRP of PFPMA are rare, owing to the high reactivity of the pentafluorophenyl (PFP) ester, which may potentially cause hydrolysis of the ester or protonation of the metal ion and the ligand.[74] In these reasons, only few studies are reported with lower molecular weight. The ATRP of less reactive 2,3,4,6-tetrafluorophneyl methacrylate (TFPMA) ester with EBiB (ethyl α–bromo isobutyrate)/CuBr/ $CuBr_2$/ 1,1,4,7,10,10-hexamethyltriethylenetetramine (HMTETA) system was reported Gan group.[75] In their studies, $CuBr_2$ was employed as a deactivator to improve kinetic control of polymerization. As far as our present knowledge goes, ATRP of PFPMA under EBiB/CuBr/N,N,N'N'',N''-pentamethyldiethylenetriamine (PMDETA) system is first result that show possibility of ATRP with PFPMA. The molecular weight, however, is limited to lower than 13 kDa with broader PDI (>1.2).[76]

Kinetic control is important to control molecular weight and PDI, which is necessary for obtain particular structure of interest such as polymer nanoparticles[77]

and brushes[78] with desired properties. Although the reactivity of PFPMA is reduced than their acrylates counterparts, it still has higher reactive with primary and secondary amine at higher temperature than 40 °C.[65] The potential of hydrolysis of monomers with linear ligands (HMTETA, PMDETA) may cause poisoning of catalyst/ligands complexes.

In this study, we reported that PFPMA could be polymerized under ATRP condition with enhanced control of kinetics, resulting enhanced features (higher molecular weight and narrow PDI) (Figure 2.3). In order to enhance the kinetic control by prevent the hydrolysis of monomer, catalyst poisoning, and termination, careful choice of ligand and catalyst were conducted with EBiB initiator in Toluene. Kinetics of polymerization were monitored by $^{1}H$ and $^{19}F$-NMR and SEC and obtained polymers were characterized with $^{1}H$ and $^{19}F$-NMR, SEC, and FT-IR.

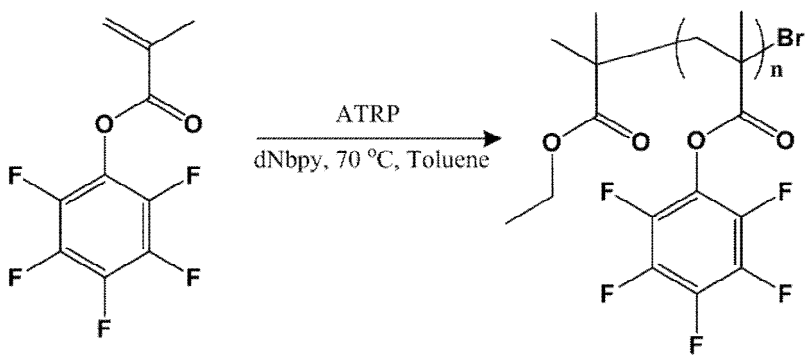


**Figure 2.3.** Synthetic scheme for ATRP of PFPMA with ethyl α-bromoisobutyrate (EBiB)/$Cu^{I}$/dNbpy system in toluene.

## 2.1. Experimental section

### Materials

Methacryloyl chlorid (>80.0%) and pentafluorophenol (99%) was purchased from Tokyo Chemical Industry Co., LTD. and Alfa Aesar, respectively. All other chemicals including initiator, solvent, ligands, Copper(I) briomide (CuBr) and Copper(I) chloride (CuCl) were purchased from Sigma-Aldrich. CuBr and CuCl were purified by stirring with acetic acid and filtered. After washing with absolute ethanol, the purified catalysts were dried and stored under vacuum. Anhydrous solvent, monomer, and initiator for ATRP polymerization was bubbled with nitrogen for 30 minute directly prior to use to remove dissolved oxygen in liquid. All other commercially available chemicals were used as received. ATRP were conducted under nitrogen atmosphere using standard Schlenk techniques.

### Characterization

NMR spectra were obtained from Bruker Avance-500 MHz and Avance-300 MHz (500 MHz for $^{1}$H-NMR, 282 MHz for $^{19}$F-NMR) spectrometer. All proton chemical shifts were referenced to residual $CDCl_3$ resonance at 7.26 ppm. Polymer molecular weights and polydispersity indices were estimated by gel permeation chromatography on YL9100 system (Young Lin Instrument Co., Ltd.), using PMMA standards for calibration and tetrahydrofuran (THF) as eluent at a

flow rate of 1mL/min at 40 °C. Infrared spectra were obtained from PerkinElmer Frontier.

### Synthesis of pentafluorophenyl methacrylate (PFPMA)

PFPMA was synthesized by nucleophilic substitution of 17.2 mL of methacryloyl chloride (0.176 mol) and 27 g of phentafluorophenol (0.147 mol) in present of 24.6 mL of triehtylamine (TEA) and 700 mL of ethyl ether as previously reported method.[79] 19 g of a colorless liquid (yield 52%) was obtained after column chromatography with hexane as an eluent.

$^{1}$H NMR ($CDCl_3$) δ: 6.43 (t, 1H, $CH_2$), 5.93 (t, 1H, $CH_2$), 2.11 (t, 3H, $CCH_3$). $^{19}$F NMR ($CDCl_3$) δ: -164.48 (dd, 2F, meta), -160.19 (t, 1F, para), -154.72 (d, 2F, ortho).

### ATRP of Poly(pentafluorophenyl methacrylate) (poly(PFPMA)

In typical ATRP polymerization, CuCl (3.4 mg, 0.0341 mmol), and 4,4'-dinonyl-2,2'-bipyridyl (dNbpy) (27.8 mg, 0.068 mmol) were added to a flame-dried Schlenk tube and sealed with a rubber septum. After the flask was evacuated and back-filled with nitrogen three times to remove oxygen, dried and deoxygenated toluene (0.14 mL) and PFPMA (1.24 mL, 6.8 mmol) were added with nitrogen-purged syringes and stirred until catalyst and ligand complex was formed. Ethyl- α-bromoisobutyrate (EBiB) (10uL, 0.068 mmol) was added after catalyst complex had formed. The reaction was conducted in an oil-bath at 70 °C

for 5 min, 15 min, 1 h, 2 h, 4 h, 6 h, 8 h, 12 h, respectively. The diluted solution was submitted to $^{19}F$ NMR measurements to determine monomer conversion by comparing of the integrated monomer resonance at -159.97 ppm and polymer resonance at 159.10 ppm. Poly(PFPMA) was purified by iterative dissolution/reprecipitaiton in THF/methanol several times.

$^{1}H$ NMR ($CDCl_3$) δ: 2.41 (br, s, 2H, $CH_2$), 1.38 (br, s, 3H, $CCH_3$). $^{19}F$ NMR ($CDCl_3$) δ: -163.98 (br, s, 2F, meta), -158.80 (br, s, 1F, para), -152.80 (br, d, 2F, ortho). FT-IR: 1780 $cm^{-1}$ (C=O stretching band of activated ester), 1523$cm^{-1}$ (C=C stretching band of aromatic group).

## 2.3 Results and discussions

### 2.3.1. Effect of catalyst on kinetics

In order to establish an optimal ATRP condition for PFPMA, hydrolysis of monomer or poisoning of catalyst and initiator should be eliminated. Reactivity between PFPMA and two different ligands, N,N,N'N'',N''-pentamethyldiethylenetriamine (PMDETA) and 4,4'-dinonyl-2,2'-bipyridyl (dNbpy), which represent linear and pyridyl-based ligand was tested. Four different samples, pure PFPMA and pentafluorophenol, mixture of PFPMA and PMDETA, and mixture of PFPMA and dNbpy, were prepared. After 12 h of reaction at 70 °C, the samples were submitted to $^{19}F$ NMR. NMR spectrum of mixture of PFPMA and PMDETA had extra peaks at -168.07 and -169.78 ppm, which were not found in those of pure PFPMA and mixture of PFPMA and dNbpy (Figure 2.4). Those extra peaks were from pentafluorophenol produced from hydrolysis of monomer. This result indicates that dNbpy is more suitable than PMDETA for ATRP of PFPMA since hydrolysis of monomer is negligible with dNbpy.

In order to optimize ATRP condition for PFPMA, series of ATRP with PFPMA were conducted under EBiB (Ethyl- α-bromoisobutyrate)/CuBr/dNbpy. Various conditions such as ratio between initiator and catalyst, kind of catalyst, concentration of solution, and reaction temperature was varied (Table 2.1). When the polymerization was conducted without toluene, high monomer conversion and

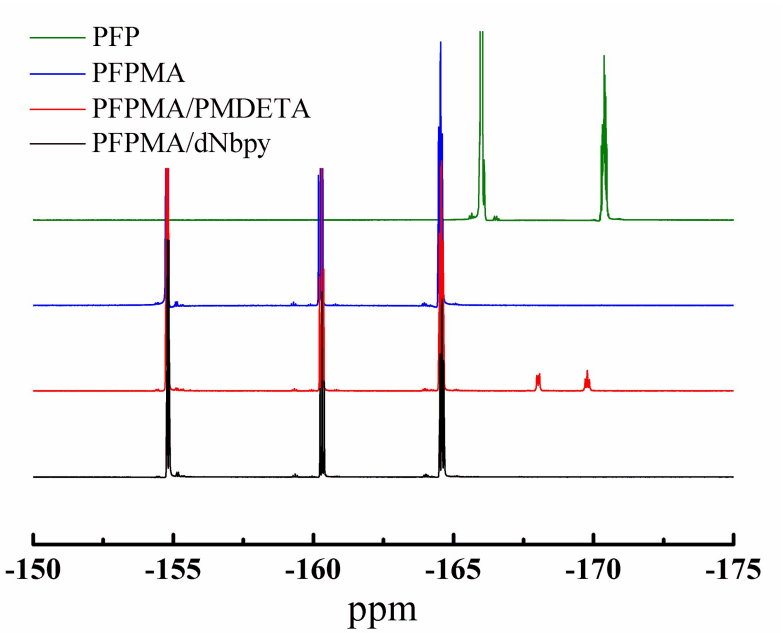


**Figure 2.4.** $^{19}F$ NMR spectra of pentafluorophenol (PFP, green line), pentafluorophenyl methacrylate (PFPMA, blue line), PFPMA with N,N,N'N'',N''-pentamethyldiethylenetriamine (PMDETA) (PFPMA/PMDETA, red line), PFPMA with 4,4'-dinonyl-2,2'-bipyridyl (dNbpy) (PFPMA/dNbpy, black line) after 12 h of reaction in pre-heated oil bath at 70 °C.

**Table 2.1.** ATRP of pentafluorophenyl methacrylate (PFPMA) using EBiB (I)/Cu-X/dNbpy (L) system (X=Br or Cl[a]) under various conditions in toluene.

| Entry | [M]/[I] | [$Cu^{(I)}$]/[I] | [$Cu^{(II)}$]/[I] | [L]/[I] | Concen-tration | Temp (℃) | Time (h) | Conv (%) | $M_{nth}$ | IE | SEC | | |
|---|---|---|---|---|---|---|---|---|---|---|---|---|---|
| | | | | | | | | | | | $M_n$ | $M_w$ | $M_w/M_n$ |
| P1 | 100 | 1 | 0 | 2 | bulk | 70 | 12 | 92 | 23197 | 76 | 30566 | 46054 | 1.51 |
| P2 | 100 | 0.5 | 0 | 1 | bulk | 70 | 12 | 85 | 21432 | 86 | 24974 | 39769 | 1.59 |
| P3 | 100 | 0.5 | 0 | 1 | 10 vol% | 70 | 12 | 84 | 21180 | 64 | 32913 | 40896 | 1.24 |
| P4 | 91 | 0.5[a] | 0 | 1 | 10 vol% | 70 | 12 | 76 | 17438 | 100 | 17596 | 20064 | 1.14 |
| P5 | 100 | 0.75 | 0.25 | 2 | 10 vol% | 70 | 12 | 78 | 19667 | 61 | 32212 | 40827 | 1.26 |
| P6 | 100 | 0.5 | 0 | 1 | 20 vol% | 70 | 12 | 74 | 18658 | 69 | 27000 | 34200 | 1.27 |
| P7 | 100 | 0.5 | 0 | 1 | 30 vol% | 70 | 12 | 47 | 11851 | 49 | 24090 | 31798 | 1.32 |
| P8 | 100 | 0.5 | 0 | 1 | 50 vol% | 70 | 12 | 35 | 8825 | 44 | 19917 | 25158 | 1.26 |
| P9 | 100 | 0.5 | 0 | 1 | bulk | 50 | 24 | 42 | 10590 | 45 | 23765 | 32800 | 1.38 |
| P10 | 100 | 0.25 | 0 | 0.5 | bulk | 70 | 12 | 69 | 17398 | 100 | 17355 | 26206 | 1.51 |

initiator efficiency (IE) were observed at 1:1 and 1:0.5 of ratio between initiator and catalyst. Broad PDI, however, indicated that kinetic control is failed under this condition. As volume percent of toluene increase, we could narrow down PDI with reduced monomer conversion and initiator efficiency. When ratio between initiator and catalyst is 1:0.5 in 10% (v/v) of toluene at 70 °C, high monomer conversion and initiator efficiency with relatively narrow PDI was observed.

We conducted kinetic studies on ATRP of PFPMA under 1:0.5 of ratio between initiator and monomer in 10% (v/v) of toluene at 70 °C. Slope of semi-logarithmic plot was proportional to concentration of growing radical ([P*]) (Equation 2.3). Thus, changes on slope of semilogarithmic plot for optimal condition with CuBr (Figure 2.5) indicates that concentration of growing radical is deceased rapidly after 30 minute. Furthermore, the number average molecular weights ($M_n$) obtained from GPC analysis were much higher than theoretical $M_n$ despite narrow PDI. Matyjaszewski group previously addressed that this result was attributed to the lower relative rate of initiation.[71] They could solved a problem by replacing CuBr with CuCl in the ATRP of PMMA. After replacing CuBr with CuCl, we also confirmed that ATRP of PFPMA showed enhanced radical control from the semilogarithmic plot and the molecular weights more similar to the theoretical values for poly(PFPMA). With optimal condition, molecular weight of poly(PFPMA) was 17 k Da and PDI was 1.14.

$$\ln\left(\frac{[M]_0}{[M]_t}\right) = \frac{k_p K_{ATRP}[P_n X]\,[Cu^{I}]}{[Cu^{II}]}\,t \qquad \text{Equation 2.3}$$

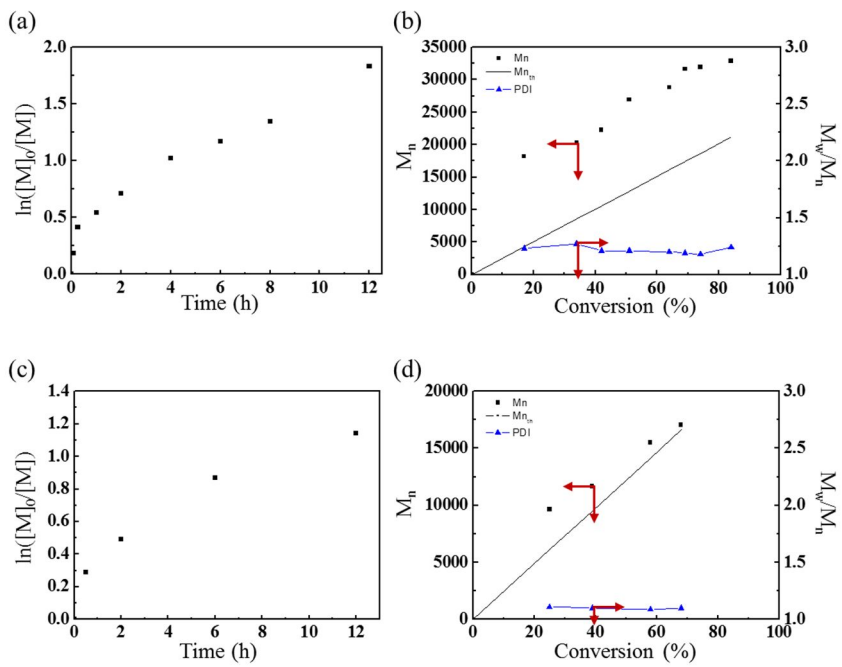


**Figure 2.5.** Semilogarithmic plot of (a, c) $\ln([M]_0/[M])$ vs time, (b, d) $M_n$ (square) and $M_w/M_n$ (triangle) vs conversion for ATRP of PFPMA at 70°C in 10 vol% of toluene. (a, b) were polymerized under CuBr, (c, d) under CuCl: $[PFPMA]_0$ = 4.97 M; $[EBiB]_0$ = 0.049 M; $[Cu(I)]_0$ = 0.024 M; $[dNbpy]_0$ = 0.049 M.

## 2.3.3. Effect of temperature on molecular weight

With optimal condition of ATRP with PFPMA in hand, higher molecular weight was tried by changing ratio between initiator and monomer from to 1:487 (Table 2.2). The kinetic studies were conducted by varying temperature from 70 °C to 110 °C. Only 24% of monomer conversion is observed with 24 h of reaction at 70 °C, while 45 % of monomer conversion with high molecular weight (63 kDa, which is higher value compared with previously reported results[76, 80]) was achieved for 24h in 90 °C. The similar monomer conversion was observed at 90 °C and 110 °C after 24 h of reaction. The tails behind main peak on GPC trace of poly(PFPMA) polymerized 110 °C, however, indicated broader PDI for poly(PFPMA) polymerized at 110 °C than 90 °C caused by termination of earlier step (Figure 2. 6). Kinetic study of ATRP with PFPMA at 90 °C was conducted. In semilogarithmic plot, concentration of active species was decreased due to the persistent radical effect (PRE),[81] especially for the chain-length-dependent PRE as molecular weight of poly(PFPMA) was increased. While polymerization rate of poly(PFPMA) was decreased, well-defined poly(PFPMA) with pre-determined molecular weight and narrow PDI was obtained. Poly(PFPMA) was characterized with $^{1}H$ NMR, $^{19}F$ NMR, and FT-IR. FT-IR indicated side reactions such as hydrolysis of monomer or substitution of ligands were negligible since absence of O-H stretching band of carboxylic acid around 3500 $cm^{-1}$ and amide bond around at 1650 $cm^{-1}$ (Figure 2.7).

**Table 2.2.** ATRP of pentafluorophenyl methacrylate (PFPMA) using EBiB (I)/CuCl/dNbpy (L) system under various temperature in 10 % (v/v) of toluene for high molecular weight.

| Entry | [M]/[I] | $[Cu^{(I)}]/[I]$ | $[Cu^{(II)}]/[I]$ | [L]/[I] | Concen-tration | Temp (℃) | Time (h) | Conv (%) | $M_{nth}$ | IE | SEC | | |
|---|---|---|---|---|---|---|---|---|---|---|---|---|---|
| | | | | | | | | | | | $M_n$ | $M_w$ | $M_w/M_n$ |
| P11 | 487 | 0.5 | 0 | 1 | 10 vol% | 70 | 24 | 27 | 33154 | 81 | 40600 | 46000 | 1.13 |
| P12 | 487 | 0.5 | 0 | 1 | 10 vol% | 90 | 24 | 45 | 55257 | 88 | 63000 | 72400 | 1.15 |
| P13 | 487 | 0.5 | 0 | 1 | 10 vol% | 110 | 24 | 47 | 57712 | 106 | 54200 | 68600 | 1.27 |

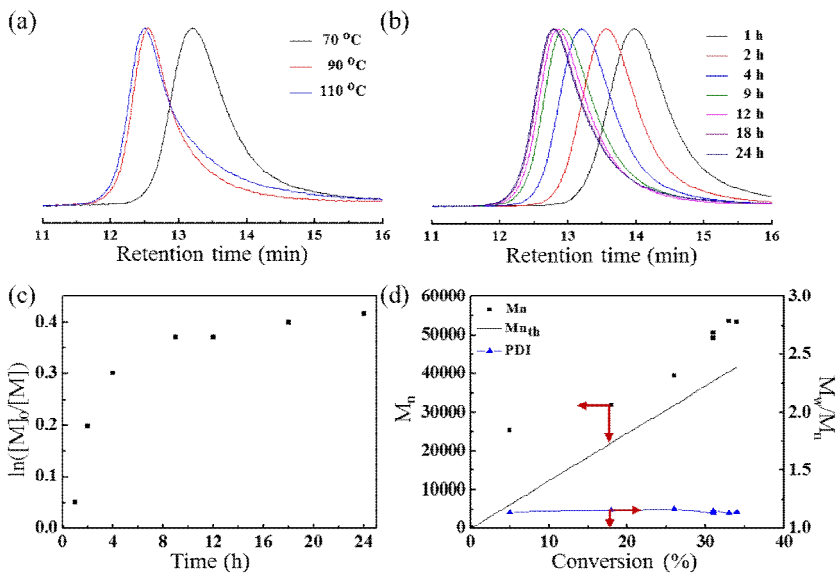


**Figure 2.6.** GPC trace of poly(PFPMA) for (a) polymerization under different temperature, and (b) polymerization at 90 °C with different time. Semilogarithmic plot of (c) $\ln([M]_0/[M])$ vs time, (d) $M_n$ (square) and $M_w/M_n$ (triangle) vs conversion for ATRP of PFPMA at 90°C in 10 vol% of toluene: $[PFPMA]_0$ = 4.97 M; $[EBiB]_0$ = 0.010 M; $[Cu(I)]_0$ = 0.005 M; $[dNbpy]_0$ = 0.010 M.

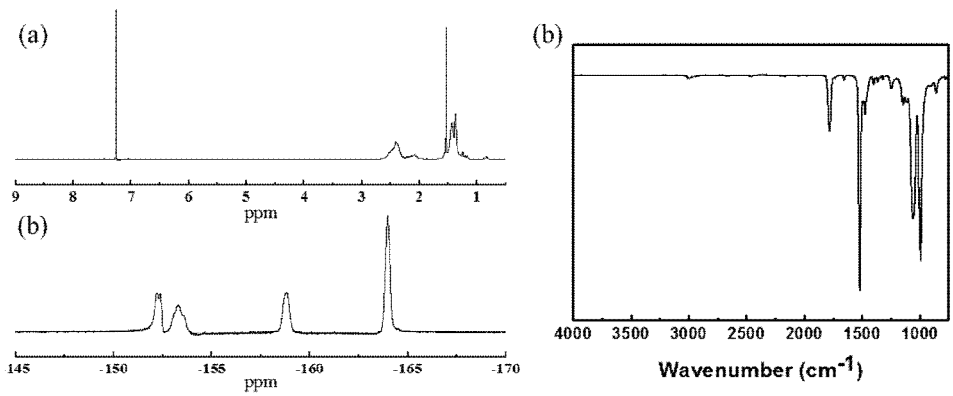


**Figure 2.7.** (a) $^{1}H$ NMR, (b) $^{19}F$ NMR, and (c) FT-IR spectra of poly(PFPMA).

## 2.4 Conclusions

The optimal condition for ATRP of PFPMA was established with EBiB/CuCl/dNbpy system in 10% (v/v) of toluene. When the ratio between initiator, catalyst, and ligand was 1:0.5:1, the resulting polymer has high monomer conversion (76%) and initiator efficiency (99%). When the ratio between initiator and monomer was 100, kinetics of polymerization was well controlled at 70 °C, resulting similar number average molecular weights ($M_n$) to theoretic value by employing CuCl instead of CuBr to increase initiate rate and decrease proportion rate. Furthermore, degree of polymerization (DP) could be increased by increasing reaction temperature to 90 °C. The efforts for choice of suitable ligand and catalyst of reaction condition and series of reaction to optimize reaction condition allowed that the polymerization was conducted without any side reaction, and resulting polymer has pre-determined molecular weight and narrow PDI.

With optimal condition for ATRP of PFPMA, we expect that ATRP will allow fine control of composition and topology of poly(PFPMA), which will act as a scaffold of functional polymer nanoparticles. Furthermore, we evaluate that this works expand window for new polymerization technique of poly(PFPMA). Thus, we can choose proper polymerization technique for particular application. In chapter 3, we will discuss about demonstration of fluorescent polymer nanoparticles (in section 3.1), and stimuli-responsive polymer nanoparticles (in section 3.2) with poly(PFPMA) polymerized with ATRP to prove merits of ATRP of poly(PFPMA) for versatile platforms.

# Chapter 3. Preparation of Reactive Polymer Nanoparticles Platforms Based on Poly(pentafluorophenyl methacrylate)

## 3.1. Synthesis of fluorescent polymer nanoparticle from poly(pentafluorphenyl methacrylate)

### 3.1.1. Introduction

With a wide range of applications such as electronics, photonics, and biotechnology,[82, 83] fluorescent nanoparticles (NPs) such as lanthanide-doped NPs,[84, 85] quantum dots (QDs),[86-88] Cornell Dots (CDs),[89, 90] and fluorescent polymer NPs[52, 91, 92] have garnered considerable interest. Among them, fluorescent PNPs merit attention because of fine tunability of its properties by careful chemical modification and free of heavy metal ions such as $Cd^{2+}$ and $Pb^{2+}$. The toxicity of those ions caused extra efforts devoted to the surface passivation and biological evaluation of QDs[93] or recent endeavors to synthesize less toxic derivatives such as InP QDs.[94-96] Furthermore, it shows relatively high quantum yields and less self-quenching than organic dyes and allows for a wide variety of chemical modification.

As already mentioned in section 1.2, polymeric NPs can be prepared from dispersion of pre-made polymers by solvent evaporation,[51], [97] emulsification,[98] nanoprecipitation,[52], [92], [99] or by the direct polymerization of monomers through emulsion,[43] miniemulsion,[100] and interfacial[101] polymerization. Among these preparation methods, nanoprecipitation is one of the most widely used methods since it allows simple and fast preparation of PNPs with surfactant-free surface,[102] which is very important for further modification of PNPs to introduce those PNPs into PNP-friendly environment. Studies on nanoprecipitation of fluorescent PNPs has been intensively achieved with fluorescent polymers including poly(p-phenyleneethynylene) (PPE),[92] poly(p-phenylenevinylene) (PPV),[103] and polyfluorene (PF).[104]

While the controlling of their photophysical properties such as emission wavelength is a very important feature of the fluorescent NPs, modular control of emission wavelength of those fluorescent conjugated polymer nanoparticles (PNPs) is relatively difficult. Cumbersome synthesis of the fluorescent conjugated polymers is also required to tune polymer's electronic structure for controlling their emissive properties. Furthermore, the surface modification of these fluorescent PNPs are difficult and requires extensive post-polymerization modification, as well demonstrated by Swager and coworkers,[92] or particle encapsulation.[105] Thus, simple and modular method for preparing fluorescent PNPs with desired emission properties are highly demanded. The issue was recently addressed by synthesizing block copolymer NPs with activated ester core and hydrophilic shell, which was

subsequently infused with amine-containing dye.[106], [107] Such method of modifying pre-formed nanostructures is intriguing and allows for a rapid formation of functional NPs, but is limited to those dyes which can permeate through the shell layer.

In this section, we demonstrated a facile approach to prepare fluorescent PNPs from reactive polymer by post-modification of poly(PFPMA) prepared by ATRP with condition optimized in chapter 2 (Figure 3.1). Nanoprecipitating the commercial dye substituted poly(PFPMA) in THF/water mixtures was conducted to evaluate the potential of using the poly(PFPMA) as a platform for loading amine-based dyes in a modular approach to yield fluorescent polymers and PNPs with desired emissive properties. By varying parameter for nanoprecipitation, average size of NPs was controlled. The size and shape were characterized by transmission electron microscopy (TEM), dynamic light scattering (DLS), and the emission properties were studied with UV-Vis and photoluminescence (PL) spectroscopy.

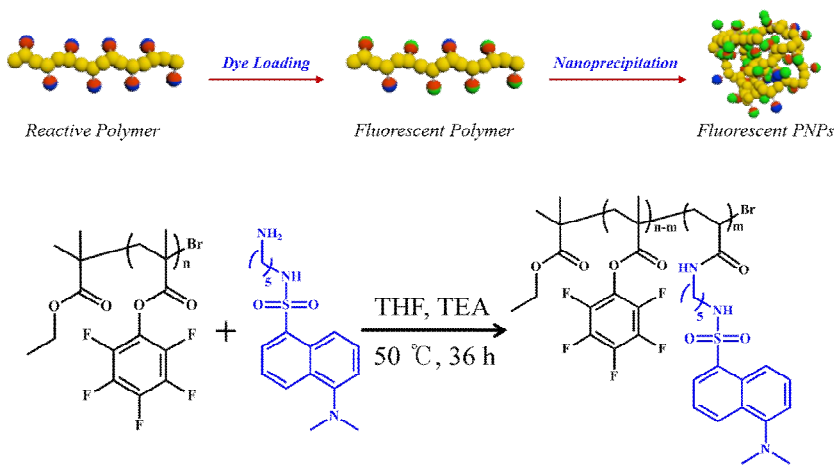


**Figure 3.1.** Schematic illustration of preparation procedure for fluorescent polymer and fluorescent PNP by post polymerization modification of poly(PFPMA) with commercial dye and subsequently nanoprecipitation.

## 3.1.2. Experimental section

### Materials and Method

All commercially available chemicals including dansylcadaverine (≥ 97%), triethylamine (99.5%), and anhydrous THF was purchased from sigma aldrich, and used as recived. Poly(PFPMA) ($M_n$=17 kDa, PDI=1.14) polymerized by ATRP was used as a scaffold. All air- and moisture-sensitive procedures were conducted under nitrogen atmosphere using standard Schlenk techniques.

### Charaterization

NMR spectra were obtained from Bruker Avance-500 MHz and Avance-300 MHz ($^1$H NMR was conducted under 500 MHz, 282 MHz for $^{19}$F-NMR) spectrometer, and all proton chemical shifts were referenced to residual $CDCl_3$ resonance (7.26 ppm). Polymer molecular weights and polydispersity indices were characterized by gel permeation chromatography on YL9100 system (Young Lin Instrument Co., Ltd), using PMMA standards for calibration and tetrahydrofuran (THF) as eluent at a flow rate of 1mL/min at 40 °C. Infrared spectra were obtained from PerkinElmer Frontier. UV-Vis absorption spectra were obtained with PerkinElmer Lambda 35 after correcting for background signal with a solvent-filled cuvette. Photoluminescence (PL) spectra were recorded from PerkinElmer LS55 using right-angle detection. Photoluminescence quantum yields were measured under optically dilute conditions,[108] using quinine sulfate in 0.1 M

$H_2SO_4$ as a reference and were corrected for solvent refractive indices and absorptivity differences at the excitation wavelength (350 nm). Dynamic light scattering (DLS) for nanoparticle size and size distribution measurements was conducted on ELSZ-1000 (Otsuka Electronics) using deionized water as solvent. Transmission electron microscopy (TEM) images were obtained on JEM1010 (JEOL) using 80 kV acceleration voltage. Spectral grade solvents were used unless otherwise noted.

**General Modification of Poly(PFPMA) with Dansylcadaverine**

Poly(PFPMA) (0.1 g, 0.40 mmol of activated ester group), and triehtylamine (0.2 mL) dissolved in 0.5 mL of anhydrous THF were placed in 3 separate 5 mL vials. 0.5 equivalent amount of dansylcadaverine (66.9 mg, 0.199 mmol) based on activate ester group were added, respectively. The mixture was placed in an oil bath pre-heated to 50 °C and allowed to stir for 36 hours. The resulting poly(pentafluorophenyl methacrylate)-*co*-poly((dansylcadaverine) methacrylamide) (p(PFPMA)-*co*-p(dansyl)) was obtained by precipitation in methanol and purified by iterative and dissolution a reprecipitation in THF and methanol, respectively. The polymer was characterized by NMR, GPC, IR, and UV-Vis and photoluminescence spectroscopy (m= 38 % where m is number of repeat units with dansylcadaverine (Figure 3.1)).

$^1$H NMR ($CDCl_3$) δ: 8.45 (br, s, 1H), 8.29 (br, s, 1H), 8.14 (br, s, 1H), 7.43

(br, s, 2H), 7.09 (br, s, 1H), 6.49 (br, s, 1H), 2.82~1.26 (br, 34H).

$^{19}$F NMR ($CDCl_3$) δ: -163.98 (br, s, 2F, meta), -158.80 (br, s, 1F, para), -152.80 (br, d, 2F, ortho).

IR: 2800~3000 $cm^{-1}$ (aromatic C-H stretching band of naphthalene), 1780 $cm^{-1}$ (C=O stretching band of activated ester), 1650 $cm^{-1}$ (C=O stretching band of amide), 1523 $cm^{-1}$ (C=C stretching band of aromatic group).

**NP Formation via Nanoprecipitation**

NP formation was conducted from a solution of 100, 50, and 10 μg of p(PFPMA)-*co*-p(dansyl) each in 1 mL of THF. The solution was mixed for overnight to make sure homogeneous solution. The copolymer solutions were filtered through 0.2 μm PFTF syringe filter and added to 9 mL deionized water under sonication at 0.05, 0.1, and 0.25 ml/min rates. The suspension was sonicated for additional 30 minutes to remove THF and subjected to dialysis against deionized water for 2 days. Clear, fluorescent dispersions were obtained and characterized by TEM, DLS, UV-Vis and photoluminescence spectroscopy.

### 3.1.3. Results and discussions

With the optimized conditions for controlled polymerization of PFPMA in hand, poly(PFPMA) with $M_n$ = 17600 g/mol (PDI = 1.14) was polymerized by ATRP. 0.5, 0.3, and 0.1 equivalent amount of dansylcadaverine (66.9 mg, 0.199 mmol/ 40 mg, 0.119 mmol/ 13 mg. 0.04 mmol) relative to number of repeating units were treated with poly(PFPMA), respectively, in the presence of trimethylamine in THF to introduced fluorescent. Dansylcadaverine, a commercially available amine-functionalized fluorophore was chosen as the model dye in the present study since its photophysical properties are sensitive to the immediate environment surrounding the molecule.[109] 38 %, 16 %, and 7% of dye conversion was observed within 36 hours for 0.5, 0.3, and 0.1 equivalent amount, respectively and the $^1$H NMR spectroscopy of the resulting polymers indicated the quantitative substitution of pentafluorophenyl moieties on the polymers based on the converted dansylcadaverine and $^{19}$F NMR spectroscopy of the resulting polymers indicated residual pentafluorophenyl ester group which may open possibility of further modification (Figure 3.2). The GPC analysis shows a slight increase in the molecular weight which was attributed to the incorporation of the large dansyl side chains and Monomodal movement of the GPC trace without the formation of a shoulder peak or a tail indicated that the dansylcadaverine substitution occurs evenly throughout the polymer chains. IR spectra of the substituted polymers showed the presence of an amide peak at 1650 $cm^{-1}$ and

multiple peaks from the aromatic C-H stretch from

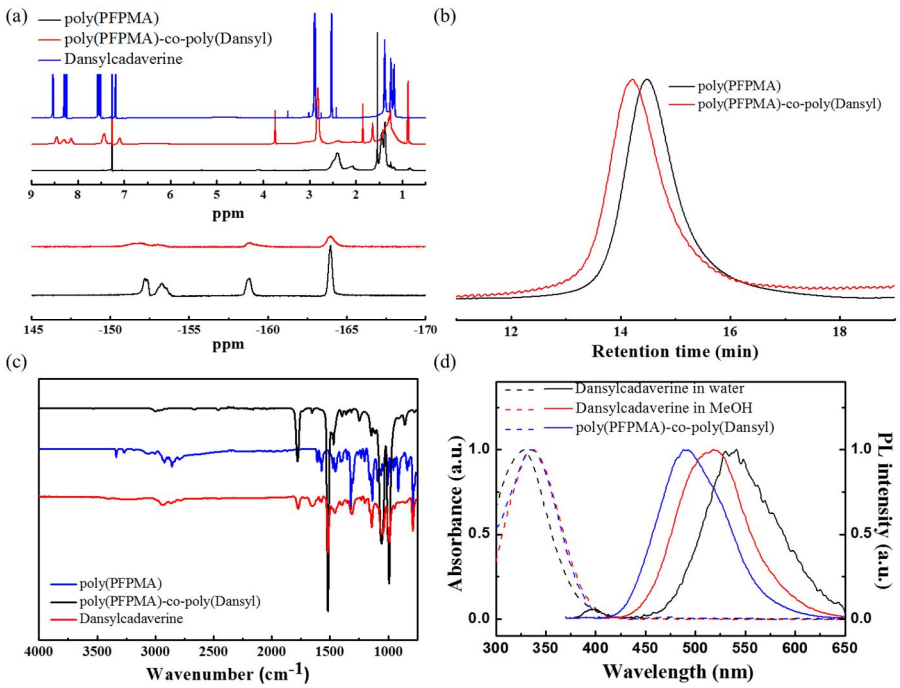


**Figure 3.2.** Post polymerization modification of poly(PFPMA) with dansylcadaverine dye. (a) $^{1}$H NMR and $^{19}$F NMR specta of poly(PFPMA), poly(PFPMA)-*co*-poly(dansyl), and dansylcadaverine. (b) GPC trace for poly(PFPMA) before and after substitution of dansylcadaverine, (c) FT-IR spectra of poly(PFPMA), poly(PFPMA)-*co*-poly(dansyl), and dansylcadaverine (d) UV-Vis (dashed line) and fluorescence spectra (solid line) of poly(PFPMA)-*co*-poly(dansyl) (blue), dansylcadaverine in MeOH (red) and water (black).

naphthalene (around 2800~3000 $cm^{-1}$) core of the dansyl unit. The hydrolysis of the PFPMA units was negligible as indicated by absence of O-H stretching band of carboxylic acid groups around 3500 $cm^{-1}$. The photoluminescence spectrum of the resulting polymer indicated that fluorescent properties of dansylcadaverine was imparted into reactive polymers.

The relative quantum yields of substituted polymers in THF was characterized to study photophysical property of substituted polymer depending on the amount of dye loading (Table 3.1). The relative quantum yields was deceased as the amount of dye loading was increased since the distance of each dye molecules was decreased, resulting energy transfer between dye molecules. It is, however, remarkable that width of decrease of substituted polymer (m=0.38, where m is number of repeat units with dansylcadaverine) was less than 13 % based on free dye molecules. Furthermore, lower quantum yield of substituted polymer with m=0.16 indicates that arrangement of dye molecules was of great concern than number of them in chain.

Since the introduction of the nanoprecipitation method by Fessi[99] in 1989, much work has been devoted to determine the effect, on the NP properties such as average size and its distribution, of concentration of polymer solution, injection rate, aqueous phase agitation rate, and the ratio between organic phase and aqueous phase.[75], [105], [110], [111] The morphology of dansyl-containing NPs was characterized by TEM depending on the concentration of polymer solution and the injection rate

(Figure 3.3). We also investigated the relationship between average sized and initial

| | **Quantum Yield (%)** | **FWHM (nm)** |
|---|---|---|
| Dansylcadaverine in THF | 41.6 | 80 |
| poly(PFPMA)-co-poly(Dansyl) in THF (m=0.38) | 36.7 | 82 |
| poly(PFPMA)-co-poly(Dansyl) in THF (m=0.16) | 29.6 | 82 |
| poly(PFPMA)-co-poly(Dansyl) in THF (m=0.07) | 39.9 | 82 |

**Table 3.1.** Relative quantum yield of substitued polymers in THF depending on the amount of dye loading.

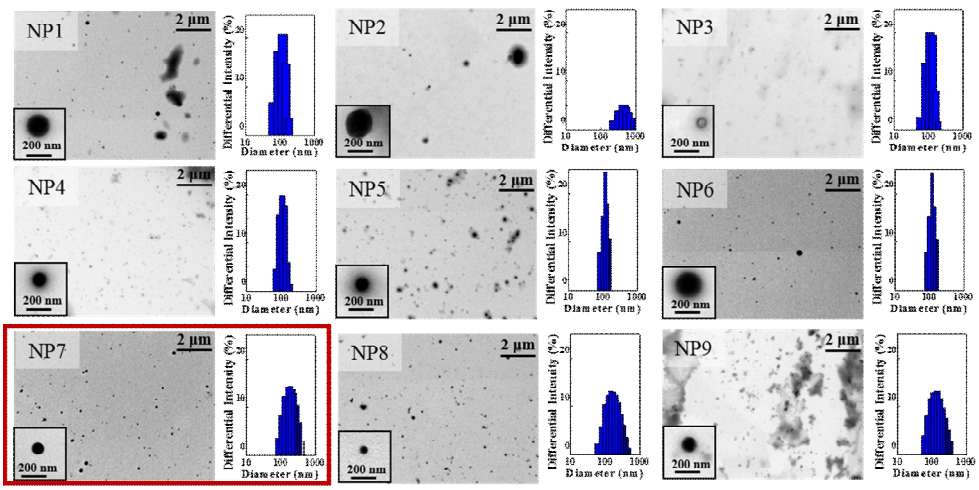


**Figure 3.3.** TEM images and DLS data of NPs from poly(PFPMA)-*co*-poly(dansyl). Injection rates are 0.05 mL $min^{-1}$ (NP 1, 4, 7), 0.1 mL $min^{-1}$ (NP 2, 5, 8), and 0.25 mL $min^{-1}$ (NP 3, 6, 9). Polymer concentrations are 10 μg $mL^{-1}$ (NP 1-3), 50 μg $mL^{-1}$ (NP 4-6), and 100 μg $mL^{-1}$ (NP 7-9).

**Table 3.2.** Average particle size of NPs from poly(PFPMA)-*co*-poly(dansyl) depending on injection rate and initial polymer concentration.[①]

| Entry | Diameter, nm (PDI) | Entry | Diameter, nm (PDI) | Entry | Diameter, nm (PDI) |
|---|---|---|---|---|---|
| NP 1 | 126.9 (0.201) | NP 4 | 113.2 (0.156) | NP7 | 180.1 (0.194) |
| NP 2 | 572.8 (1.287) | NP 5 | 78.8 (0.107) | NP8 | 163.2 (0.187) |
| NP 3 | 124.6 (0.177) | NP 6 | 128.5 (0.131) | NP9 | 132.6 (0.203) |

[①]Injection rates are 0.05 mL $min^{-1}$ (NP 1, 4, 7), 0.1 mL $min^{-1}$ (NP 2, 5, 8), and 0.25 mL $min^{-1}$ (NP 3, 6, 9). Polymer concentrations are 10 μg $mL^{-1}$ (NP 1-3), 50 μg $mL^{-1}$ (NP 4-6), and 100 μg $mL^{-1}$ (NP 7-9).

concetration and injection rate by varying concentration of polymer solution (10, 50, 100 μg $mL^{-1}$) and injection rate (0.05, 0.1, 0.25 mL $min^{-1}$). Average particle size measured by DLS was summarized in table 3.2. The tendency depending on initial concentration and injection rate is well matched with previously reported result. By increasing the initial concentration of polymer solution, average particle size was observed to increase.[77], [110] Furthermore, smaller particles were obtained when the injection rate, aqueous phase agitation rate, and the relative volume of the aqueous phase were increased.[77] The most well-defined particles with 180 nm of hydrodynamic diameter obtained when a polymer solutions of higher concentration (100 μg $mL^{-1}$) was added at a slower rates (0.05 mL $min^{-1}$) was chosen for further studies.

The photophysical properties of dansylcadaverin in water and methanol, poly(PFPMA)-*co*-poly(dansyl) in THF, and polymer NPs dispersed in water were studied by comparing relative quantum yields of them with photoluminescence spectrum (Table 3.3). The photoluminescence spectrum of the resulting polymer was blue-shifted with a slight decrease in the full width at half maximum (FWHM) compared to that of dansylcadaverine in water because of solvent effect. Furthermore, the quantum yield of the substituted polymers in THF was enhanced by a factor of nearly 2 relative to the dansylcadaverine solution in methanol and nearly by a factor of 19 relative to its solution in water, indicating the reduction of vibrational energy loss of the dye molecules upon incorporation into the polymer chain. The photoluminescence spectrum of polymer NPs dispersed in water did not

show noticeable changes when compared with the polymer dissolved in THF (Figure 3.4). The quantum yields of NPs were found to be lower by a factor of about 4.2 when compared with that of the polymer in THF, an observation which could be attributed to the formation of dye aggregates upon nanoprecipitation.[91], [112], [113] This number is comparable to the results from McNeil group[52] which reported a 4-fold decrease for poly(9,9-dihexylfluorenyl-2,7-diyl) (PFO), 7-fold decrease for poly[{9,9-dioctyl-2,7-divinylene-fluorenylene}-*alt-co*-{2-methoxy-5-(2- ethylhexyloxy)-1,4-phenylene} (PFPV) and a 25-fold decrease for poly[2-methoxy-5-(2-ethylhexyloxy)-1,4-phenylenevinylene] (MEH-PPV) upon nanoprecipitation. The quantum yields of the fluorescent NPs with different amount of dye loading, however, was significantly enhanced by a factor of 2 ~ 4.5 fold depending on amount of dye loading when compared with dansylcadaverine in water, indicating the potential utility of the method in achieving fluorescent polymer NPs with excellent emissive properties in water (Table 3.4).

Photo stability of polymer NPs in water was studied by comparing change of fluorescent intensity with dansylcadaverine under UV irradiation (20kW, Xenon flash lamp) (Figure 3.5). Fluorescent intensity of polymer NPs was slow decreased down to 86 % for 1800 s while that of dansylcadaverine was rapidly decreased for 500 s down to 30%. This results indicates that photo stability of polymer NPs were ensured by preventing contact of water through encapsulating dye molecules with polymer chain. As a results, the dispersion of NPs in water was

stable for more than two weeks, and their fluorescence properties such as emission spectrum and quantum yield did not show any significant change.

**Table 3.3.** Relative quantum yield of dansylcadaverine, poly(PFPMA)-*co*-poly(dansyl), and polymer NPs.

| | $\lambda_{em}$ (nm) | Quantum Yield (%) | FWHM (nm) |
|---|---|---|---|
| Dansylcadaverine in water | 541 | 1.9 | 84 |
| Dansylcadaverine in MeOH | 520 | 18.3 | 51 |
| poly(PFPMA)-*co*-poly(Dansyl) in THF | 489 | 36.7 | 82 |
| Polymer NP1[②] in water | 485 | 8.6 | 80 |
| Polymer NP2[③] in water | 485 | 3.8 | 84 |
| Polymer NP3[④] in water | 392 | 0.15 | N.A |

② concentration of polymer solution is 100 μg $mL^{-1}$ and injection rate is 0.05 mL $min^{-1}$.

③ concentration of polymer solution is 50 μg $mL^{-1}$ and injection rate is 0.1 mL $min^{-1}$.

④ concentration of polymer solution is 10 μg $mL^{-1}$ and injection rate is 0.1 mL $min^{-1}$.

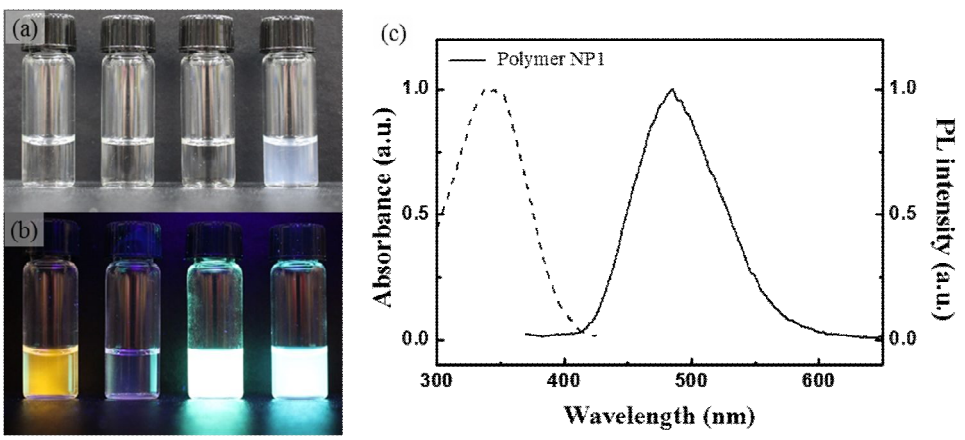


**Figure 3.4.** Photographs of solutions (left to right) of dansylcadaverine in water, poly(PFPMA) in THF, poly(PFPMA)-*co*-poly(dansyl) in THF, and polymer NP1 in water. (a) under room light and (b) under illumination with hand-held UV lamp (365 nm). (c) The UV-Vis (dashed line) and fluorescence spectra (solid line) of polymer NP1 in water.

**Table 3.4** Relative quantum yield of polymer NPs dispersed in water depending on the amount of dye loading.

| | **Quantum Yield (%)** | **FWHM (nm)** |
|---|---|---|
| Dansylcadaverine in water | 1.9 | 84 |
| PNP (m=0.35) in water (size = 180 nm) | 8.56 | 80 |
| PNP (m=0.16) in water (size = 205 nm) | 4.89 | 83 |
| PNP (m=0.07) in water (size =198 nm) | 3.79 | 90 |

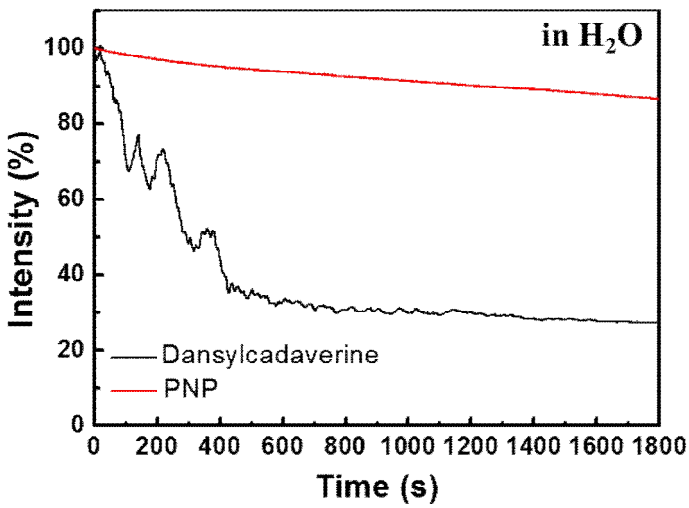


**Figure 3.5** Photostability study of polymer NPs and dansylcadaverine in water.

### 3.1.4 Conclusions

We have developed a simple, two-step approach for preparing well-defined fluorescent polymer NPs from reactive polymer. The procedure involves the modification of poly(PFPMA) with commercial dyes and subsequently nanoprecipitating the material in THF/water mixtures. Substitution with a model fluorescent dye, dansylcadaverine, proceeded smoothly to yield blue-fluorescent polymers which were then transformed into NPs by the nanoprecipitation from THF/water mixtures. By controlling the initial polymer solution concentration and the injection rate, particle size could be varied, and well-defined NPs with relatively low size distribution were obtained. Furthermore, the NPs dispersed in water showed the 4.5-fold increase in the quantum efficiency and enhanced photo stability when compared with the free dye molecules in water.

The results constitutes a highly promising system towards a facile and modular synthesis of fluorescent polymer NPs, the fluorescent properties of which could be tuned by simply choosing fluorophores with desired properties. In additon, the possibilty of reactive polymer as a platform for functional polymers was evaluated. Investigaton of stimuli-responsive polymer NPs based on obtained knowledges in this section, along with the further modification of NPs with residula PFP groups (details in section 3.2).

## 3.2. Modular synthesis of functional polymer nanoparticles from a versatile polymer nanoparticles (PNP) platform

### 3.2.1. Introduction

During the past decades, the interest in functional polymer nanoparticles has been increased due to their wide range of applications.[114-116] Many types of polymer nanoparticles featuring interesting properties, such as biocompatibility,[103], [117] stimuli responsiveness,[15], [118] and fluorescence[92], [100] have been demonstrated. While PNPs with different structure and properties have been reported, tedious synthesis and post-polymerization modifications were often required to realize PNPs with desired functions. Zentel and co-workers have recently reported cationic nanogel for siRNA delivery applications.[106] The nanogel was obtained from the self-assembly of amphiphilic diblock copolymer containing an amine-reactive block followed by core cross-linking through diamine treatment. While this approach provides a promising reactive ester platform for various biological applications,[119] multi-step polymerization and assembly are required. Furthermore, surface functionalization of the nanogels is difficult. Similar PNP platforms based on diamine cross-linked amine-reactive copolymer nanogels[120] or self-assembled amphiphilic aggregates based on an amine containing random[121] have been introduced by Thayumanavan and co-workers as a platform for multifunctional

PNPs. The method is limited to copolymers with certain composition of monomers since their nanoaggregate formation depends on hydrophilic/liophilic balance of amphiphilic random copolymers. Furthermore, the approach involves diamines and ammonium ions which are known for potential cytotoxicity.[122], [123] A novel method, therefore, which allows for a rapid and modular preparation of structurally stable, functional PNPs, independent of polymer composition, is of interest.

Activated ester monomers and their polymers could be promising scaffold for simplifying preparation methods of PNPs and for their subsequent modification.[21], [79], [124] In section 3.1, we demonstrated functional polymer nanoparticles with fluorescence for a model study to evaluate the possibility of facile synthesis of functional polymer nanoparticles, involving substitution/nanoprecipitation of poly(PFPMA) for a facile preparation of fluorescent PNPs in a surfactant free environment.[80] Further modification, however, had been difficult due to the dissolution of nanoprecipitated PNPs in various organic solvent, limiting the types of molecules which could be loaded onto the particles.

Photochemical reaction is one of the useful strategy among intra-chain crosslinking[125] including dynamic bonding,[126] polymerizations,[127], [128] click chemistry[44] since light allows remote localization without destruction and reactions under ambient temperature.[129], [130] Various photochemical active moieties such as anthracene,[131], [132], [133] cinnamic acid,[134] coumarin,[130], [135] thymine,[136] and stilbene[137] have been extensively studied to demonstrate photo-

resists, nanoparticles, self-healing materials, and photoresponsive polymers since those moieties are able to undergo photo-reversible dimerization proceed by either a [4π+4π]- or [2π+2π]-cycloaddition mechanism and allows facile control of degree of dimerization(DD).[129] Among those photochemically active functional groups, coumarin moieties have been attracted for both inter-[138] and intra-[139] particle crosslinking in functional polymer nanoparticles.

In this section, we demonstrate a strategy for a facile preparation of various functional PNPs through reactive PNP platforms based on coumarin-modified poly(PFPMA) (poly(PFPMA)-*co*-poly(CMA)) (Figure 3.6).[140] Nanoprecipitation was chosen since it allows for a facile and rapid preparation of polymer nanoparticles with little dependence on the overall polymer composition, and, importantly, can be easily converted to a continuous process.[138] The crosslinking of PNPs, obtained from the nanoprecipitation, through photo-dimerization of coumarin groups, imparted structural stability even in the presence of good solvents for the parent polymer. Furthermore, the residual activated ester groups made possible further modification of the particle with not only small molecules such as isopropylamine, *N*-(2-aminoehtyl)-3-(3',3'-dimethyl-6-nitrospiro[chromene-2,2'-indolin]-1'yl) propanamide (spiropyran-amine), or dansylcadaverine, but also with amine terminated poly(N-isopropylacrylamide) (poly(NIPAAM)), resulting in PNPs which show thermo-, and photo- response or fluorescence. The functional PNPs were characterized by transmission electron microscopy (TEM), dynamic light scattering (DLS), and UV-Vis and

photoluminescence (PL) spectroscopy.

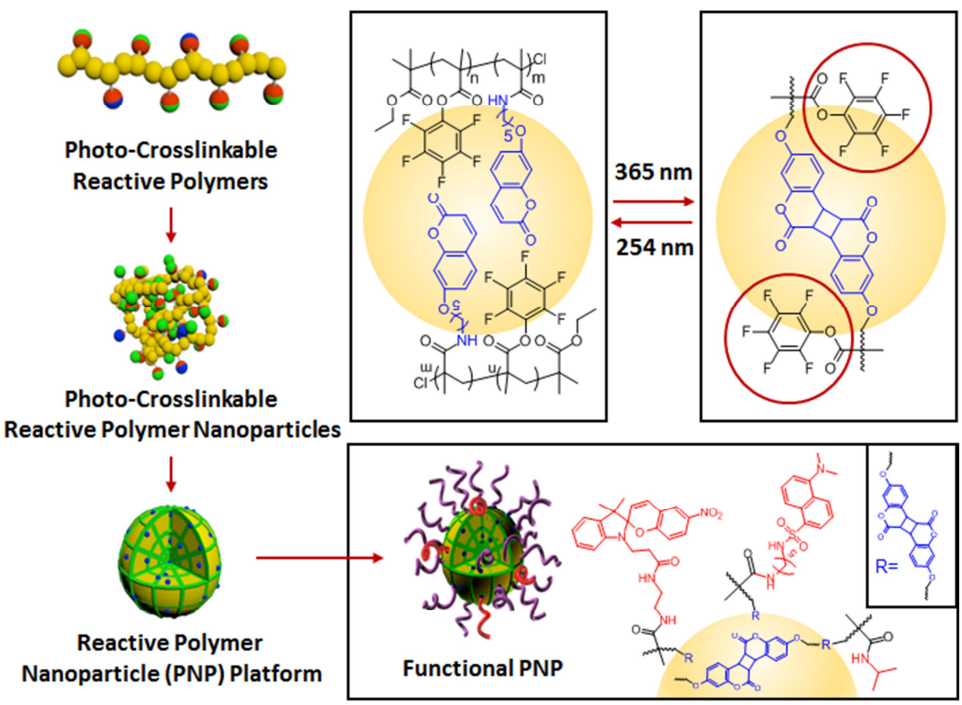


**Figure 3.6.** Schematic illustration for the preparation of functional PNPs from versatile platform based on poly(pentafluorophenyl methacrylate).

## 3.2.2. Experimental section

### Materials

7-hydroxycoumarin (98%), *N*-(5-bromopentyl)phthalimide (97%) were purchased from Alfa Aesar and all other chemicals and solvents were purchased from Sigma-Aldrich. Anhydrous toluene and THF were distilled over sodium/benzophenone and stored over 4Å molecular sieves. All other commercially available chemicals were used as received.

### Characterizations

NMR spectra were obtained from Bruker Avance-500 MHz and Avance-300 MHz ($^{1}$H NMR was conducted under 500 MHz, 282 MHz for $^{19}$F-NMR) spectrometer, and all proton chemical shifts were referenced to residual $CDCl_3$ resonance (7.26 ppm) and DMSO-$d^6$ resonance (2.54 ppm). GC-MS was characterized using JMS-600W. Polymer molecular weights and polydispersity indices were estimated by gel permeation chromatography on YL9100 system (Young Lin Instrument Co., Ltd), using PMMA standards for calibration and tetrahydrofuran (THF) as eluent at a flow rate of 1mL/min at 40 ℃. Infrared spectra were obtained from PerkinElmer Frontier. UV-Vis absorption spectra were obtained with PerkinElmer Lambda 35 after correcting for background signal with a solvent-filled cuvette. Photoluminescence (PL) spectra were recorded from PerkinElmer LS55 using right-angle detection. Photoluminescence quantum yields

were measured under optically dilute conditions,[108] using quinine sulfate in 0.1 M $H_2SO_4$ as a standard and were corrected for solvent refractive indices and absorptivity differences at the excitation wavelength (350 nm). Dynamic light scattering (DLS) for nanoparticle size and size distribution measurements was conducted on ZEN 3690 (Malvern) using deionized water as solvent. Transmission electron microscopy (TEM) images were obtained on JEM1010 (JEOL) using 80 kV acceleration voltage. Spectral grade solvents were used unless otherwise noted.

**Synthesis of N-(2-aminoehtyl)-3-(3',3'-dimethyl-6-nitrospiro[chromene-2,2'-indolin]-1'yl) propanamide (spiropyran-amine)**

Spiropyran-amine was synthesized according to previously reported procedure.[19].

$^1$H NMR (DMSO-$D_6$) δ: 8.20 (d, 1H), 7.98 (dd, 1H), 7.18 (d, 1H), 7.10 (m, 2H), 6.84 (d, 1H), 6.66 (t, 1H), 5.96 (d, 1H), 3.87 (d, 1H), 3.72 (t, 1H), 3.00 (m, 2H), 2.35 (m, 4H), 1.24 (s, 3H), 1.16 (s 3H), 1.05 (s, 2H).

ESI mass spectra: 425.3 (2.04%), 424.2 (16.37%), 423.2 (100.0%), 276.2 (3.08%), 275.2 (2.04%), 274.2 (6.83%).

**Synthesis of 7-((5-aminopentyl)oxy)-coumarin (coumarin-amine)**

7-((5-aminopentyl)oxy)-coumarin) (coumarin-amine) synthesized by nucleophilic substation of 7-hydroxycoumarin and *N*-(5-bromopentyl)phthalimide and deprotection of phthalimide according to previously reported procedures[141]

[142]

$^{1}$H NMR ($CDCl_3$) δ: 8.36 (br, s, 3H), 7.62 (d, 1H), 7.34 (d, 1H), 6.82 (dd, 2H), 6.23 (d, 1H), 4.02 (t, 2H), 3.08 (t, 2H), 1.85 (m, 4H), 1.62 (m, 1H).

FAB mass spectra: m/z 248.1, MW 248.3, 248.1 (100%), 249.1 (16.05%), 250.1 (1.80%), 251.1 (0.15%), 252.1 (0.01%).

**Substitution of 7-((5-aminopentyl)oxy)-coumarin into poly(PFPMA) (poly(PFPMA)-*co*-poly(CMA))**

7-((5-aminopentyl)oxy)-coumarin (90 mg, 0.317 mmol), poly(PFPMA) (0.1 g, 0.0049 mmol), and trimethylamine (0.2 mL) were dissolved in 1 mL of anhydrous acetone. The reaction was conducted in 50 °C oil bath for 48 h. The resulting copolymer was isolated by precipitation in methanol and purified by iterative dissolution/reprecipitation in THF and methanol, respectively. The polymer was charaterized by NMR, GPC and IR.

$^{1}$H NMR ($CDCl_3$) δ: 7.62 (br, 1H), 7.34 (br, 1H), 6.82 (br, 2H), 6.23 (br, 1H), 4.02 (br, 2H), 3.08 (br, 2H), 2.41~1.38 (br, 16H).

$^{19}$F NMR (CDCl3, δ): -163.98 (br, s, 2F), -158.80 (br, s, 1F), -152.80 (br, d, 2F)

FT-IR: 2800~3000 $cm^{-1}$ (aromatic C-H stretching band of naphthalene), 1780 $cm^{-1}$ (C=O stretching band of activated ester), 1650 $cm^{-1}$ (C=O stretching band of amide), 1523 $cm^{-1}$ (C=C stretching band of aromatic group).

**Nanoparticle formation**

NP formation was conducted from a solution of 100, and 50 μg of poly(PFPMA)-*co*-poly(CMA) each in 1 mL of THF. The solution was mixed for overnight to make sure homogeneous solution. The copolymer solutions were filtered through 0.45 μm PFTF syringe filter and added to 9 mL deionized water under sonication at 0.05, 0.1, and 0.25 ml/min rates. The suspension was sonicated for additional 30 minutes to remove THF and subjected to dialysis against deionized water for 2 days. Clear, fluorescent dispersions were obtained and characterized by TEM, DLS, UV-Vis and photoluminescence spectroscopy as according to previously reported procedure.[80]

**Photo dimerization of nanoparticle and kinetic study**

For the spectroscopic studies on photodimerization, optically dilute samples (O.D. =0.02~0.05), prepared by the dilution of nanoprecipitated particles dispersion with water, in quartz glass cell (1 cm X 1 cm) were irradiated with a hand lamp (4W) under 365 nm and 254 nm for dimerization and cleavage, respectively. Distance between UV lamp and cell was fixed with 3 cm. 200 μL of sample was taken and diluted with 3 mL of DI-Water to measure excitation intensity at time t in optically diluted condition.

**Modification of reactive polymer nanoparticle (PNP) platform:**

Solution of cross-linked PNP in THF (0.01 mg/mL, 1 mL each) were placed in 4 separate 5 mL vials. Isopropylaime (0.2 mL), spiropyran-amine (20 mg), dansylcadaverine (20 mg), and amine terminated poly(NIPAAm) ($M_n$=2500, 50 mg) were then added into vials, separately. After 0.2 mL of triethylamine was added to each reaction mixture, the solutions were placed in an oil bath pre-heated at 50 °C. The reaction mixtures were then allowed to stir for 48 h followed by dialysis against distilled water (10,000 molecular weight cut-off) for one week to remove residual amines. Dialysis bath was charged with clean distilled water every 12 h for first two days, and 24 h for the next 5 days. To obtain the optimally dispersed solutions, solvent for each sample was then changed by changing the solvent against which dialysis was conducted. For isopropylamine and poly(NIPAAm)-treated PNPs, distilled water was used and for spiropyran-treated PNPs, DMSO was used.

### 3.2.3. Results and discussions

Activated ester containing polymer was prepared by atom transfer radical polymerization (ATRP) with pentafluorophenylmethacrylate (PFPMA) under CuCl/dNbpy catalyst system[80] as optimized in chapter 2. The obtained polymer ($M_n$=20600 g $mol^{-1}$, PDI=1.16, DP=82) was treated with 0.8 equivalent, based on total number of repeat units, of 7-((5-aminopentyl)oxy)-coumarin) (coumarin-amine) synthesized according to previously reported procedures.[141], [142] $^1H$ and $^{19}F$ NMR measurement indicated that 62% of pentafluorophenyl units were substituted to coumarin (77% efficiency) (Figure 3.7). FT-IR spectrum of substituted polymer confirmed that, based on formation of amide peak at 1650 $cm^{-1}$ and absence of carboxylic acid O-H stretch band around 3500 $cm^{-1}$, the pentafluorophenyl groups were successfully replaced with coumarin moiety without hydrolysis of unreacted penfafluorophenyl esters. The UV- Vis absorption and photoluminescence spectra of resulting polymer dispersed in THF also indicated the presence of coumarin.

Reactive PNP were then prepared by nanoprecipitation of a THF solution of poly$(PFPMA)_{31}$-*co*-poly$(CMA)_{51}$ into water. The nanoparticles exhibited well-defined spherical morphology (Figure 3.8). Effects of various nanoprecipitation parameter, such as polymer concentration and injection rate, on the size and size distribution of resulting particles were studied. It was determined, through DLS measurements, that the average hydrodynamic diameter of nanoparticles decreased with decreasing polymer concentration and increasing

injection rate (Figure 3.9).[112]

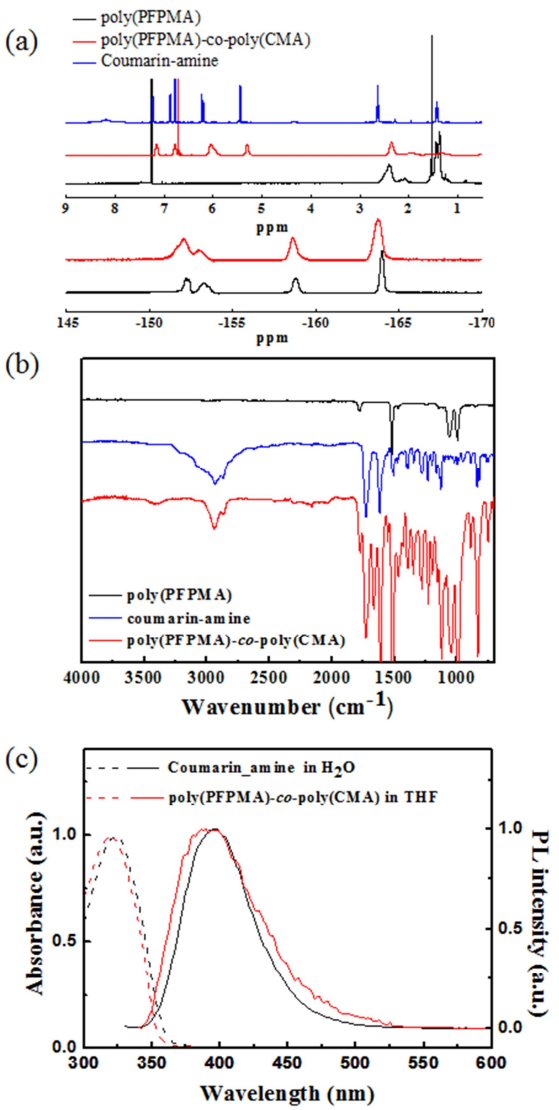


**Figure 3.7.** (a) $^{1}$H-NMR and $^{19}$F NMR spectra, (b) FT-IR of coumarin-amine (blue), poly(PFPMA) (black), and poly(PFPMA)-*co*-poly(CMA) (red), and (c) UV-vis (dashed line) and fluorescent (solid line) spectra of coumarin-amine (black) and poly(PFPMA)-*co*-poly(CMA) (red).

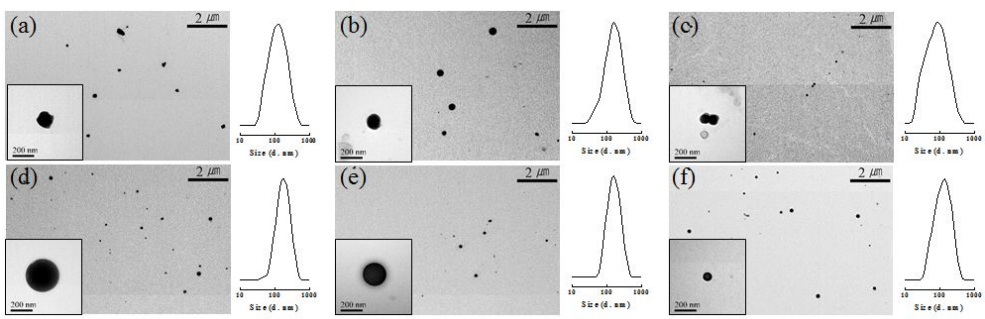


**Figure 3.8** TEM images and DLS data of the nanoprecipitated poly(PFPMA)-*co*-poly(CMA) cast from water. Polymer concentrations are 50 μg $mL^{-1}$ (a-c) and 100 μg $mL^{-1}$ (d-f). Injection rate are 0.05 mL $min^{-1}$ (a, d), 0.1 mL $min^{-1}$ (b, e), and 0.25 mL $min^{-1}$ (c, f).

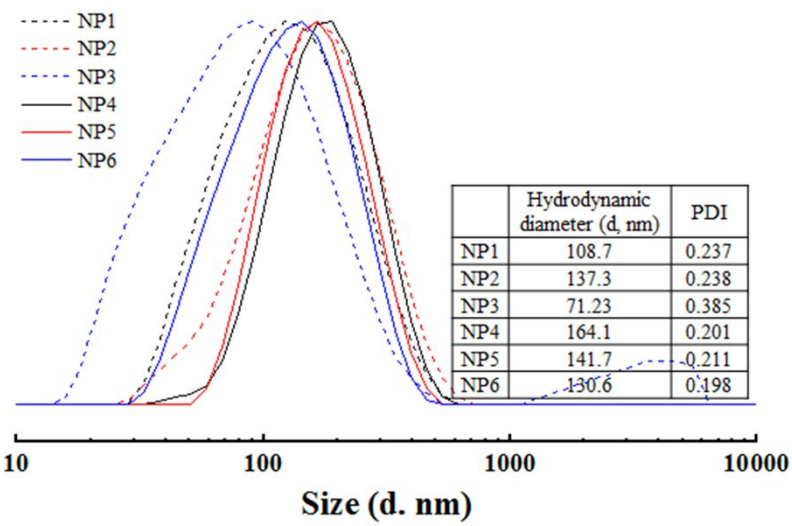


| | Hydrodynamic diameter (d, nm) | PDI |
|---|---|---|
| NP1 | 108.7 | 0.237 |
| NP2 | 137.3 | 0.238 |
| NP3 | 71.23 | 0.385 |
| NP4 | 164.1 | 0.201 |
| NP5 | 141.7 | 0.211 |
| NP6 | 130.6 | 0.198 |

**Figure 3.9** DLS intensity of polymer nanoparticles from coumarin substituted poly(PFPMA). Polymer concentrations are 50 μg $mL^{-1}$ (NP1-3) and 100 μg $mL^{-1}$ (NP4-6). Injection rate are 0.05 mL $min^{-1}$ (NP1, 4), 0.1 mL $min^{-1}$ (NP2, 5), and 0.25 mL $min^{-1}$ (NP3, 6).

**Table 3.5**. Relative quantum yield of Coumarin-amine, poly(PFPMA)-*co*-poly(CMA), and polymer NPs.

| | $\lambda_{em}$ (nm) | Quantum Yield (%) | FWHH (nm) |
|---|---|---|---|
| Coumairn-amine in water | 396 | 38.7 | 58 |
| poly(PFPMA)-*co*-poly(CMA) in THF | 390 | 1.03 | 87 |
| Polymer NP3[⑤] in water | 326 | 1.05 | 90 |
| Polymer NP6[⑥] in water | 326 | 1.71 | 81 |

⑤ concentration of polymer solution is 50 μg $mL^{-1}$ and injection rate is 0.25 mL $min^{-1}$

⑥ concentration of polymer solution is 100 μg $ml^{-1}$ and injection rate is 0.25 mL $min^{-1}$

This tendency signified the ability to effectively control the size of nanoparticle without changing the molecular weight[143] of the used polymer or fine tuning of amount of surfactant.[102] The resulting particles had hydrodynamic diameter ranging 75 nm to 165 nm and could be imaged clearly through TEM, presumably due to the high contrast provided by the presence of fluorine atoms. The particles with average diameter of 130 nm was chosen for further studied since they displayed most well-defined morphology with narrowest size polydispersity and had the highest quantum yields of coumarin emission (Table 3.5).

Photo-induced crosslinking of the reactive PNP platforms were conducted through photo dimerization of coumarin units under UV irradiation. In order to understand photochemical behaviour of coumarin, changes of absorbance of coumarin-amine in water, poly(PFPMA)-co-poly(CMA) in THF, and PNP in water upon UV irradiation was monitored (Figure 3.10). Most of cuomarins were dimerized in 4 h for coumarin-amine in water, while copolymer in THF did not for 22h because of solvent effect on photodimerization of coumarin.[144] We also found that absorbance in PNP upon UV irradiation time is hide under light scattering of particles.

Thus, monitoring change of absorbance is not proper to study photochemical behaviour of reactive PNP platforms. By monitoring changes of excitation intensity at 326 nm (Figure 3.11), the degree of dimerization (DD) of coumarin was obtained following the modified equation based on previous report,[132] $DD=(1-Ex_t/Ex_0)\times100$, with $Ex_0$ and $Ex_t$ being the initial excitation

intensity and the

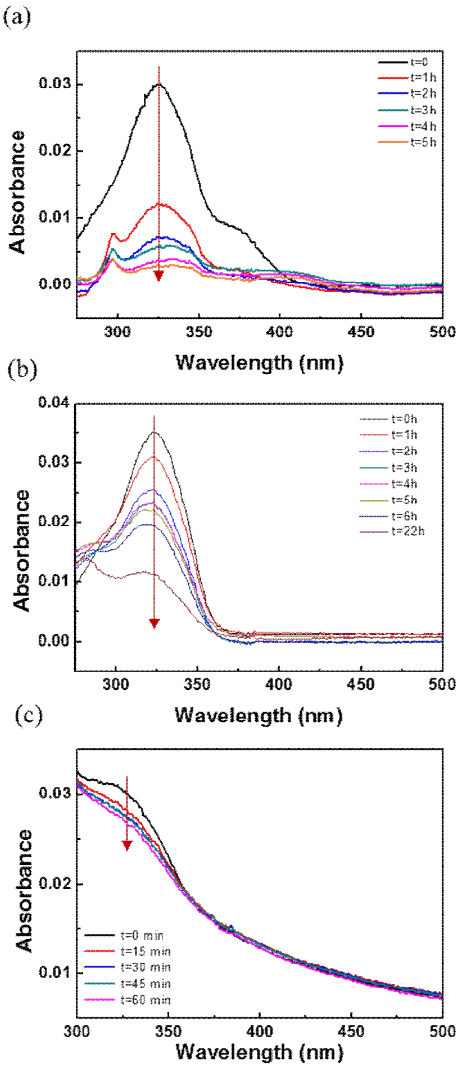

**Figure 3.10.** Absorbance changes of (a) coumarin-amine in water, (b) poly(PFPMA)-*co*-poly(CMA) in THF, and reactive PNP platform in water upon UV irradiation at 365 nm

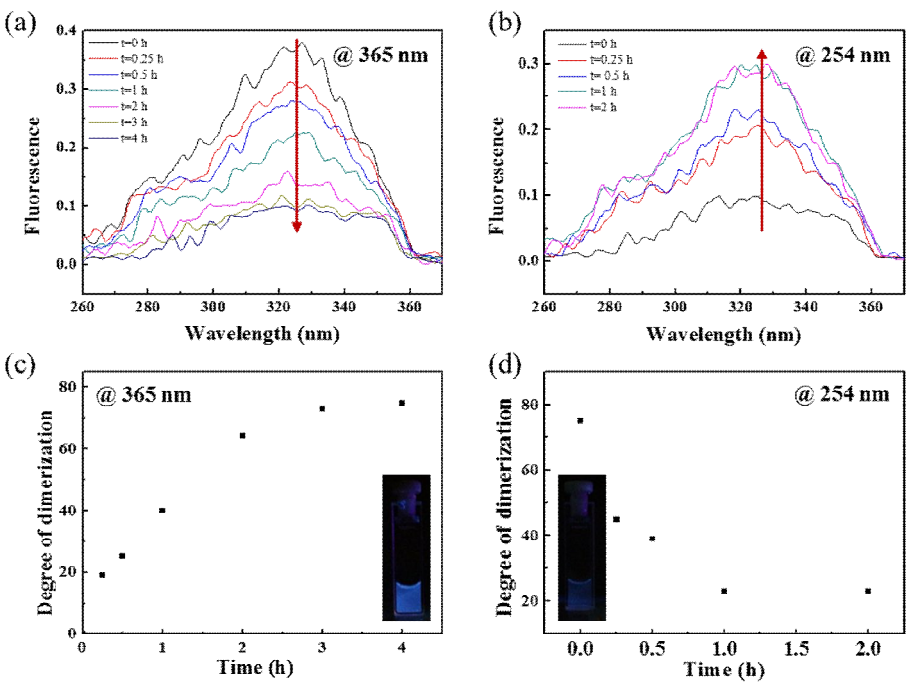


**Figure 3.11.** Excitation intensity of polymer nanoparticles upon UV irradiation at (a) 365 nm and (b) 254 nm, degree of dimerization (DD) change with time upon

irradiation at (c) 365 nm and (d) 254 nm, respectively, with the inset showing the image of the PNP solution under irradiation with a hand-held UV lamp.

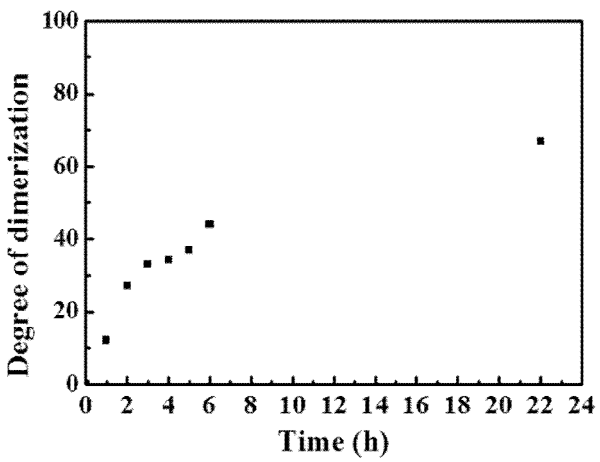


**Figure 3.12.** Degree of dimerization of poly(PFPMA)-*co*-poly(CMA) in THF.

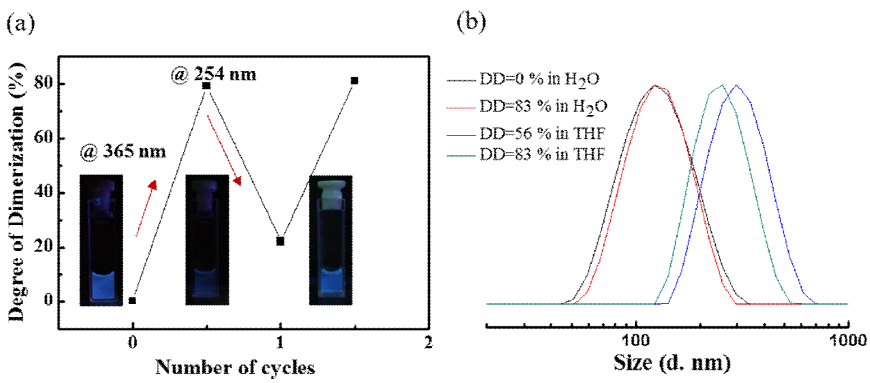


**Figure 3.13.** (a) Changes in DD with alternating irradiation at 365 nm and 254 nm, respectively, with the inset showing the image of the PNP solution under irradiation with a hand-held UV lamp, and (c) dynamic light scattering (DLS) trace (based on relative intensity) of particles with various values of DD in water and in THF.

excitation intensity after irradiation time t. After 4 hours of irradiation at 365 nm (4W), the dimerization proceeded to give a DD value of approximately 80%, for the nanoprecipitated poly(PFPMA)-*co*-poly(CMA) in water compared to 34% of poly(PFPMA)-*co*-poly(CMA) for 4h (67% for 22h) in THF (Figure 3.12). The difference was attributed to the proximity of coumarin moieties in the confines of the PNPs and solvent effect on photodimerization of coumarin.[144] The cleavage reaction of coumarin dimers was much faster than dimerization, and the DD was reduced to approximately 20% upon irradiation at 254 nm (4W) for 1h. The reversibility of dimerization and cleavage was studied by DD upon alternating UV irradiation at 365 nm and 254 nm, respectively (Figure 3.12). This result is consistent with the previous reports showing the presence of a photostationary between the coumarin monomer and the dimer upon irradiation at 254 nm.[121] DD was enabled to control by changing wavelength of UV irradiation (Figure 3.13). DLS measurements at DD=0 and 83% indicated that inter particle crosslinking was negligible. When the nanoparticles with DD=83% was exposed to THF, which is a good solvent for the free poly(PFPMA)-*co*-poly(CMA) (and a good solvent for polymer nanoparticles with DD=0), an increase in hydrodynamic diameter was observed without significant changes in their polydispersity, suggesting swelling, rather than dissolution, was occurring. The degree of swelling was closely related to the DD, with PNPs having DD=56% and 83% showing hydrodynamic diameters of 289 nm and 225 nm, respectively, in THF. For the nanoparticles with DD below approximately 50 %, no discernable intensity distributions were obtained from

DLS, suggesting that the particle dissolution is occurring at the low DD values. The results indicate that the photo-induced cross-linking of the nanoprecipitated poly(PFPMA)-*co*-poly(CMA) produced PNPs which maintain their nanoparticle structure even in a strong solvent for their uncrosslinked precursor nanoparticles. Such structural stability in THF allowed for a wide range of amines to be employed in the subsequent modification of the cross-linked nanoparticles.

With structurally stabilized reactive PNP platform at hand, the possibility of particle functionalization was probed through their treatment with two different amines containing small molecules and an amine-terminated polymer. The cross-linked poly(PFPMA)-*co*-poly(CMA) particles with DD=78% was used in the studies. When the PNPs were treated with isopropylamine, the resulting nanoparticles, poly(NIPMAM)-NP, were obtained with hydrodynamic diameter of about 190 nm at room temperature, compared to the 130 nm of the unmodified PNPs. Upon increasing the temperature, the hydrodynamic diameter of poly(NIPMAM)-NP showed a sharp drop at 40-50 °C to about 167 nm (Figure 3.14a). The observation was consistent with the known LCST behaviour of poly(*N*-isopropylmethacrylamide) (poly(NIPMAM)), which is known to undergo significant conformational changes at 45 °C.[17], [21], [79] Thermal decomposition or hydrolysis could be outruled since the unmodified cross-linked poly(PFPMA)-*co*-poly(CMA) NPs did not show variations in hydrodynamic diameter up to 70 °C . The results indicated that the treatment of the PNPs with isopropylamine leads to the facile transformation of their structure with poly(NIPMAM)-like structures,

imparting thermal responsiveness to the

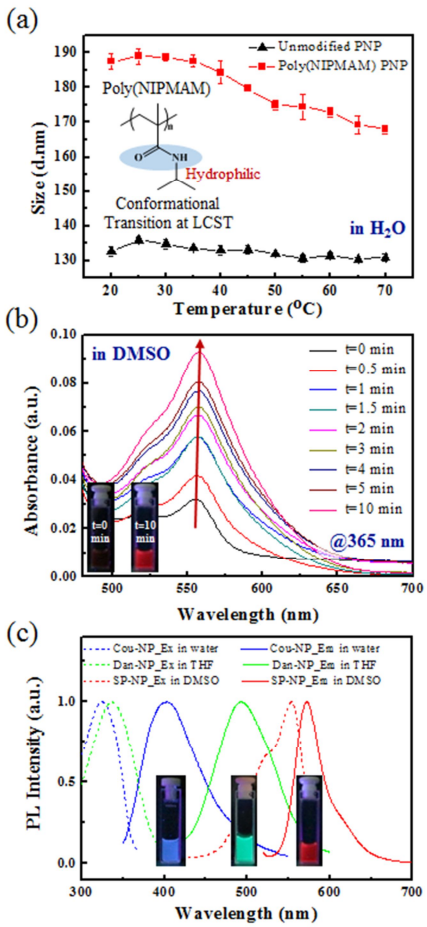


**Figure 3.14** Functionalization of reactive PNP with small molecules. (a) hydrodynamic diameter of poly(NIPMAM)-PNPs (square) and untreated reactive PNPs (triangle) at various temperatures, as determined through DLS, (b) Time-dependent changes in the absorption spectrum of spiropyran-treated reactive PNPs (SP-PNPs) upon irradiation at 365 nm, and (c) RGB fluorescence spectra (excitation (dashed line) and emission (solid line)) of coumarin (blue),

dansylcadaverine (green), and spiropyran (red) treated PNPs in water, THF, and DMSO, respectively.

particles.

The cross-linked PNPs were also treated with *N*-(2-aminoehtyl)-3-(3',3'-dimethyl-6- nitrospiro[chromene-2,2'-indolin]-1'yl) propanamide (spiropyran-amine).[145] The spiropyran moiety is a well-known chromophore that change structure from spiropyran to merocyanin upon UV irradiation at 365nm[19] and emit red fluorescent (575 nm) upon the structural transformation. The PNPs treated with spiropyran-amine (SP-PNPs) were exposed under UV light to test their photo-responsiveness. Irradiation of SP-PNPs at 365 nm, led to an increase in their absorbance at 550 nm (Figure 3.14b). The resulting PNPs showed red fluorescence upon irradiation, whereas the unmodified PNPs showed no fluorescence. This demonstrated that the PNPs could be easily modified with a photo-responsive dye with emission properties that could be controlled through irradiation.

We also investigated the possibility of simple control of emission wavelength by varying the dye with which the nanoparticles were modified. The nanoprecipiated poly(PFPMA)-*co*-poly(CMA) PNP before dimerization, SP-PNPs, and dansylcadaverine-treated reactive PNPs (Dan-PNPs) were compared (Figure 3.14c).[80] PL studies of those PNPs showed blue, red, and green emission, respectively, indicating that multicolor nanoparticles could be obtained by simple changes in the dye choice. Furthermore, the TEM images (Figure 3.15) of poly(NIPMAM)-PNPs, SP-PNPs, and Dan-PNPs in their good solvent showed the PNPs maintained well-defined morphology even after modification.

In order to establish a more general applicability of the particles

modification, the cross-linked PNPs were also treated with an amine terminated polymer poly(NIPAAm) with an $M_n$ of 2500 (poly(NIPAAm)2500-PNP). The variable temperature DLS measurements on poly(NIPAAm)2500-PNP featured drastic increase on the hydrodynamic diameter from 270 nm to over 1 μm accompanied by a sharp drop in transmittance (at 500 nm) 100% to below 1.0% upon increasing temperature from 30-40 °C (Figure 3.16). The changes could also be visually checked, with poly(NIPAAm)2500-PNP dispersions becoming very turbid at LCST (35 °C) of poly(NIPAAm) (Figure 3.16, inset).[146] Identical thermal treatment of the free amine-terminated poly(NIPAAm) showed very different intensity distributions in DLS, suggesting that the drastic changes were due to the poly(NIPAAm) bound on the PNPs (Figure 3.17). The observation indicated that poly(NIPAAm)-PNP prepared by "grafting to" method underwent inter-particle aggregation, rather than intra-particle aggregation (collapse),[147] which was in contrast to poly(NIPMAM)-PNP which showed partial particle collapse (Figure 3.14a).

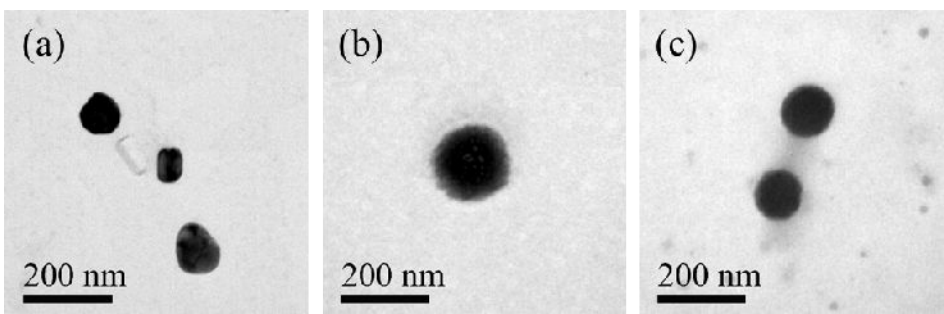


**Figure 3.15.** TEM images of (a) isopropyamine-treated PNPs (Poly(NIPMAM)-PNPs), (b) spiropyran treated PNPs (SP-PNPs), and (c) dansylcadaverine treated PNPs (Dan-PNPs).

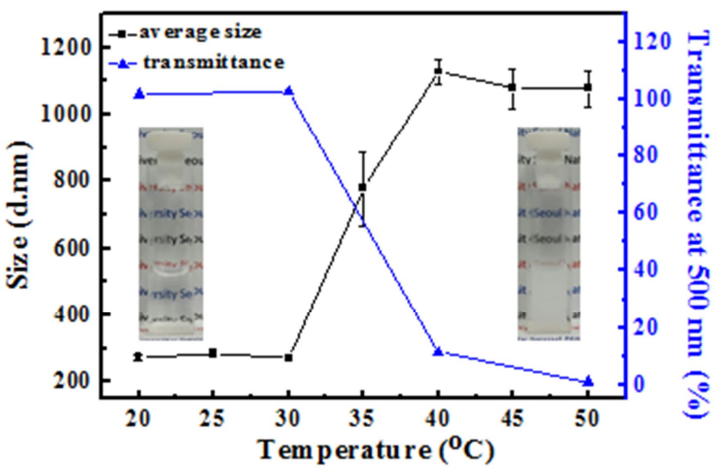


**Figure 3.16** Hydrodynamic diameter (square) and transmittance at 500 nm (triangle) of poly(NIPAAm)2500-PNPs at various temperatures, as determined through DLS an UV-vis spectroscopy, respectively, with the respective photographs added in the insets.

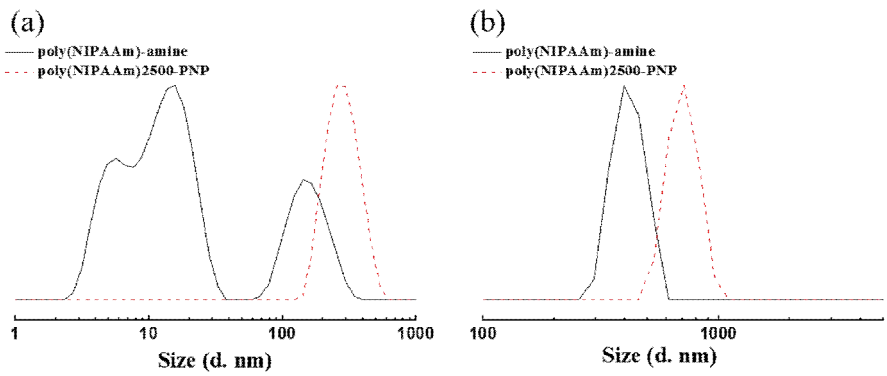


**Figure 3.17** DLS data of free poly(NIPAAm)-amine (black, solid line) and poly(NIPAAm)-PNP (red, dashed line) at (a) 20 $^{o}$C and (b) 40 $^{o}$C

## 3.2.4. Conclusions

In conclusion, facile synthesis of structurally robust, reactive PNPs platforms were achieved from a simple substitution/nanoprecipitation/photo-crosslinking strategy from poly(PFPMA). The particle size and function could be controlled by simply changing nanoprecipitation parameters and the choice of amine modifiers, respectively. Furthermore, various functional PNPs including temperature- and light-responsive PNPs, and fluorescent PNPs were prepared from the same platform by simple modification. The modifier was not limited to small molecules, and an amine-terminated polymer could be used to prepare an all polymer core-shell nanoparticles. We believe that our system and the strategy used for its achievement constitutes a useful approach that provides a facile process towards not only stimuli-responsive PNPs but also towards general advanced functional PNPs.

# Chapter 4. Preparation of Functional Polymer Brush Platforms via Surface Initiated Atom Transfer Radical Polymerization

## 4.1. Introduction

### 4.1.1 Polymer brushes

Polymer brushes are functional polymer chains tethered, at one end, to an interface or a solid surface.[148] Polymer brushes can be prepared by physiosorption or chemiosorption of polymer chain by a "grafting to" method or "grafting from method" which is that polymer grows from surface. When the polymer chains are grown from initiator on the surface, polymer brushes are of special interest since the polymer brushes with high areal density can be obtained, resulting extraordinary behavior such as extreme chain stretching due to steric repulsion.[149], [150] Such unique property has been applied extensively in areas such as antibacterial surface,[57] cell adhesion,[151] protein immobilization,[152] biosensor[153], [154] in molecular biology, macro-initiator for complex structure, responsive polymer,[155], [156] charge transfer layer[157], [158] in materials, and electronic applications depending on functionality.

The structure of a surface-immobilized polymer can be evaluated by the

inverse value of the distance between grafting points (D) and film thickness (h)

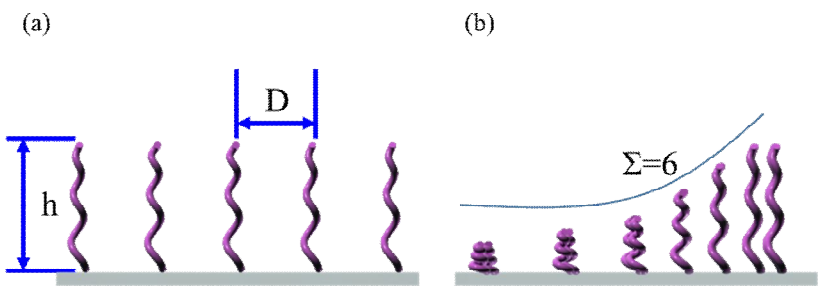


**Figure 4.1.** (a) Characteristic parameters of the polymer brush, where h is thickness, d is distance between grafting points. (b) Transition between the "mushroom" regime and "true brush" regime observed in the experiment with a grafting density gradient of polyacrylamides brushed reported by Genser et al.[160] These illustrations were reconstructed from S. Minko et. al.[159]

(Figure 4.1).[159] The point where the size of grafted polymer chains approaches the distance between grafting points is called as a transition point between a single grafted chain (mushroom) regime and brush regime. A commonly used literature parameter for quantitative characterization of this transition is the reduced tethered density (Σ) or more simply grafting density (σ), defined as equation (4.1and 4.2). [149]

$$\Sigma = \sigma \pi R_g^2 \qquad \text{Equation 4.1}$$

$$\sigma = (h\rho N_A)/M_n \qquad \text{Equation 4.2}$$

Where $R_g$ is radius of gyration of a tethered chain at specific experimental conditions of solvent and temperature, h is film thickness, ρ is bulk density of the brush composition, and $N_a$ is Avogadro`s number. Literature grafting density of high-density brushed is around 0.7, it of semi-dilutes brush is 0.05, and it of mushroom is less than 0.01.[149]

Surface initiated polymerization of brushes were demonstrated by various controlled radical polymerization techniques such as ATRP,[161] RAFT,[162] ROMP,[163] NMP[164] (most notably atom transfer radical polymerization, ATRP) to achieve maximum control over grafting density, polydispersity, and composition (block, grafting copolymer). General procedure for surface initiated controlled

radical polymerization include modification of surface of substrate with anchoring group (i.e., thiols on gold,[165] silanes on glass or Si wafer,[166] phosphorionic acid on ITO[37]) bearing initiator by self-assembled monolayer or micro-contact printing (μCP), polymerization by exposing to solutions containing components for polymerization (i.e., monomer, catalyst). Detail theories and procedure for ATRP will be discussed in 4.2.1.

Polymer brushes with desire functions can be realized by surface initiated polymerization of functional monomers or post polymerization of pre-polymerized polymer brushes. The former required difficult and cumbersome synthesis of monomers and is often tedious for optimizing polymerization conditions for each monomer. Furthermore, some functional monomers have limitation on polymerization because of tolerance as already mentioned in section 2.1. Thus, the latter is of special interest as platforms for various functional brushes. To date, modifiable brushes containing hydroxyl-, carboxylic acid-, and carboxylic ester-groups have been reported. Those functional groups, however, can be only modified with limited chemicals under harsh or toxic environment and have limitation on conversion and control.

In order to overcome those limitation, H.-A. Klok and co-workers reported RAFT polymerization of poly(pentafluorophenylmethacrylate) (poly(PFPMA)) and reactivity studies with amine containing different functional molecules.[167] In their studies, conversion of post-polymerization modification of poly(PFPMA) was achieved more than 85% for various amines (containing

functions) expect aniline which had been reported as non-reactive molecules with PFPMA.[65] Char and co-workers also reported preparation of poly(pentafluorophenyl acrylate) (poly(PFPA)) polymerized by RAFT from triethoxylsilane-containing chain transfer agent (CTA) and demonstrated fluorescent and photo-responsive surface by treating poly(PFPA) with 5-((2-Aminoethyl)amino)naphthalene-1-sulfonic acid (EDANS) and *N*-(2-aminoehtyl)-3-(3',3'-dimethyl-6-nitrospiro[chromene-2,2'-indolin]-1'yl) propanamide (spiropyran-amine), respectively.[168] The polymer brushes of poly(*N*-hydroxysuccinimide-4-vinyl benzoate) (poly(NHS4VB)) and poly(PFPA) polymerized by ATRP and free radical polymerization, respectively, from silicon wafer were reported by J. Locklin and co-workers.[169] In their study, reactivity of poly(NHS4VB) with amine is 2 orders of magnitude slower than that of poly(PFPA).[169] While those polymer brushes platform with pentafluorophenyl group showed relatively high reactivity than *N*-hydrosuccinimide based polymer, it is limited on free radical polymerization and RAFT polymerization, which have limitation on radical control (i.e., composition, molecular weight, polydispersity index) and mechanical problem based on chain transfer, causing steric hindrance of large volume of polymer chain for high molecular weight.

### 4.1.2 Surface-initiated atom transfer radical polymerization (SI-ATRP)

With an advantage of ATRP system that facile functionalization of target substrates using commercially available chemicals (i.e., α–haloester, or benayl halides), eliminating the multistep synthesis necessary for functional alkoxyamines (for NMP) and dithioesters (for RAFT),[170] ATRP system has been most actively studied to realize polymer brushes with various compositions and functions with desired architectures from both organic and inorganic materials, with either flat or curved surfaces. In earlier stage of studies on surface initiated (SI)-polymerization, termination reaction of intermolecular couplings of growing radicals, however, was often occurred because of very low concentrations of initiating groups on surface to reversible trap the propagating radicals after initiating step. By employing persistent radical (deactivator, i.e., $Cu^{II}$, $Fe^{III}$) [171] or sacrificial initiator,[78] this main challenge could be effectively solved.

In this paper, we will focus on the addition of sacrificial initiators into ATRP mixture with substrates because of its benefits in synthesis and characterization of polymer brushes. Matyjaszewski and co-worker proved that addition of sacrificial initiators into system enhanced radical controllability during polymerization.[78] Furthermore, analysis of polymer such as monomer conversion and molecular weight is greatly facilitated by analyzing free polymers formed in

solution due to a reasonable correlation between molecular weight and polydispersity for free polymer and the tethered polymer,[172], [173] allowing pre-determined molecular weight by changing the ratio between initiator and monomer in initial solution.

Features of polymer brushes are strongly affected by grafting density, which can be controlled by initiator concentration on surface, initiation efficiency, and radical control. The height measurement by ellipsometery, small angle X-ray scattering, or AFM measurement of patterned brushes is necessary to calculate grafting density. Depending on properties of substrate, careful choice of measurement technique is required.

Based on these background literature researches, we demonstrated reactive polymer brush platform based on poly(PFPMA) for electrical applications. Indium tin oxide (ITO) was used as an substrate (Figure 4.2) since it is mostly used for electric devices such as display, touch panel, solar cell, and organic light emitting diode (OLED). Prepared poly(PFPMA) brushes was treated with 4-amino-2,2,6,6,-tetramethylpiperidine 1-oxyl (4-amino-TEMPO) which are known for reversible redox electrochemical property with long term stability to investigate the possibility on preparation of surface with electrochemical properties. Control of grafting density was studied by varying concentration of initiator solution for self-assembled monolayer (SAM) of ITO. The prepared free polymers were isolated and characterized by $^{1}H$, $^{19}F$ NMR, and SEC to monitor conversion, molecular weight and polydispersity. Polymer brushes and 4-amino TEMPO treated polymer

brushes are characterized by FT-IR, X-ray photoelectron spectroscopy (XPS), and contact angle for surface chacracterization, and AFM for height.

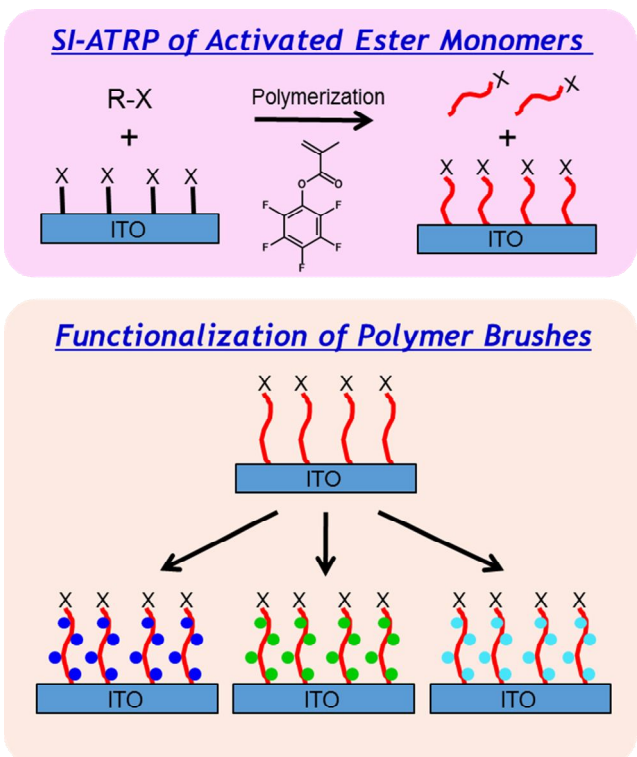


**Figure 4.2.** Schematic illustration of preparation procedure for brush platform based on SI-ATRP of PFPMA.

## 4.2. Experimental section

**Materials:**

4-amino-2,2,6,6,-tetramethylpiperidine 1-oxyl was purchased from Tokyo Chemical industry Co., Ltd and ITO glass was obtained from Kuramoto Co., Ltd. All other chemicals and solvents were purchased from Sigma Aldrich. Anhydrous toluene and THF were distilled over sodium/benzophenone and stored over 4Å molecular sieves. PFPMA was synthesized according to previously reported procedures.[79] Inhibitors of methyl methacrylate (MMA) purchased from Sigma Aldrich was removed by alumina column. Synthesis of 6-(2-bromo-2-methylpropanoyloxy)hexylphosphonic acid (surface initiator), ITO treatment and surface initiator immobilization was processed by previously reported procedure.[40] Copper(I) chloride (CuCl) were purified by stirring with acetic acid and filtering, followed by washing with absolute ethanol and drying overnight under vacuum. Solvent, monomer, and initiator for ATRP polymerization were degassed via bubbling with nitrogen for 30 minute directly prior to use. All other commercially available chemicals were used as received.

**Characterizations:**

NMR spectra, SEC data, and FT-IR spectra were obtained by previously reported method.[80] NanoWizard3 (JPK) was used for height measurement using ACTA-SS-50 (AppNano) cantilever. For electron paramagnetic resonance CW

EPR spectra (X-band; ca. 9.4 GHz) were measured with a Miniscope MS 300 instrument at 77 K cooled by liquid nitrogen in a finger Dewar (Magnettech GmbH, Berlin, Germany). Settings were as follows: center field, 2499.01 G; modulation amplitude, 2000 mG; receiver gain, 0.5; microwave attenuation, 10 dB; sweep time, 60 s. g values are referenced to external $Mn^{2+}$ in ZnS (g = 2.118, 2.066, 2.027, 1.986, 1.946, 1.906). Simulations of EPR spectra were performed with the EasySpin (v 4.0.0)69 for MatLab (R2007b).

**Surface initiated ATRP of MMA from modified ITO (ITO-g-PMMA):**

Surface initiated ATRP of methyl methacrylate (MMA) was conducted with CuCl (6.8 mg, 0.0682 mmol), and 4,4'-dinonyl-2,2'-bipyridyl (dNbpy) (55.6 mg, 0.136 mmol) were added to a flame-dried Schlenk tube with initiator immobilized ITO and sealed with a rubber septum. After the flask was evacuated and back-filled with nitrogen three times to remove oxygen, dried and deoxygenated toluene (0.48 mL) and MMA (3.5 mL, 32.64 mmol) were added with nitrogen-purged syringes and stirred. Ethyl- α-bromoisobutyrate (EBiB) (10uL, 0.068 mmol) was added after catalyst complex had formed. The reaction was conducted in an oil-bath at 70 °C for 12h. Poly(PFPMA) was purified by iterative dissolution/reprecipitaiton in THF/methanol several times to submitted to SEC. The ITO glass was rinsed with THF several times and sonicated for 15 min in THF, toluene and ethanol.

$^1$H NMR ($CDCl_3$) δ: 3.8 (br, 3H, -$COOCH_3$), 2.41 (br, s, 2H, $CH_2$), 1.38 (br, s, 3H, $CCH_3$).

**Surface initiated ATRP of PFPMA from modified ITO (ITO-g-poly(PFPMA)):**

In typical surface initiated ATRP of PFPMA, CuCl (3.4 mg, 0.0341 mmol), and 4,4'-dinonyl-2,2'-bipyridyl (dNbpy) (27.8 mg, 0.068 mmol) were added to a flame-dried Schlenk tube and sealed with a rubber septum. After the flask was evacuated and back-filled with nitrogen three times to remove oxygen, dried and deoxygenated toluene (0.67 mL) and PFPMA (6 mL, 33.2 mmol) were added with nitrogen-purged syringes and stirred. Ethyl- α-bromoisobutyrate (EBiB) (10uL, 0.068 mmol) was added after catalyst complex had formed. The reaction was conducted in an oil-bath at 90 °C for 24h. The diluted solution was submitted to $^{19}F$ NMR measurements to determine monomer conversion by comparing of the integrated monomer resonance at -159.97 ppm and polymer resonance at 159.10 ppm. Poly(PFPMA) was purified by iterative dissolution/reprecipitaiton in THF/methanol several times. The ITO glass was rinsed with THF several times and sonicated for 15 min in THF, toluene and ethanol.

$^1H$ NMR ($CDCl_3$) δ: 2.41 (br, s, 2H, $CH_2$), 1.38 (br, s, 3H, $CCH_3$).

$^{19}F$ NMR ($CDCl_3$) δ: -163.98 (br, s, 2F, meta), -158.80 (br, s, 1F, para), -152.80 (br, d, 2F, ortho). FT-IR: 1780 $cm^{-1}$ (C=O stretching band of activated ester), 1523$cm^{-1}$ (C=C stretching band of aromatic group).

**Modification of ITO-g-poly(PFPMA) with 4-amino TEMPO:**

ITO-g-poly(PFPMA) was immersed in 1wt% of 4-amino TEMPO in

anhydrous THF in present triethylamine and placed in in oil bath pre-heated at 50 °C. Reactions were conductied for 48 h. The modified ITO-g-poly(PFPMA) (ITO-g-poly(TEMPO)) was rinsed with THF and sonicated 1 min in THF and dry under innert gas.

FT-IR: 1650 $cm^{-1}$ (C=O stretching band of amide)

## 4.3 Result and discussion

### 4.3.1. SI-ATRP of PMMA with different patterning technique

In order to characterize polymer brushes by calculating grafting density, height (h) measurement is essential. Since ITO is heterogeneous for composition and its surface is very rough,[174] ellipsomtry and small angle X-ray scattering is not suitable for measuring height of polymer brushes on ITO. Thus, AFM could be solution for measuring height of polymer brushes on ITO. In order to use AFM for height measurement, selective growing of polymer chain from surface is needed. Pyun et. al. reported that selective degradation of alkyl halides was achieved by UV irradiation with TEM grid as a shadow mask.[37]

As we already discussed in previous chapter, control of grafting point (D) is important to obtain high-density polymer brushes. Thus, concentration of initiator on surface, initiation efficiency, and growing radical control are very important. R. Berger et. al. reported enhanced photo patterning technique using gold mask.[175] They could enhanced selectivity of photo degradation of polymer matrix using gold mask, which is made by sputtering of Cr and Au, sequentially. AFM measurement show clear edge of polymer matrix.

Comparison of grafting density of surface initiated PMMA (ITO-g-PMMA) with two different ITO substrates patterned with TEM grid and gold shadow mask was conducted to optimize pattering technique (Figure 4.3). Surface

initiated ATRP of PMMA was conducted with [I]:[M[:[CuCl]:[dNbpy]= 1:480:1:2 in oil bath at 70 °C for 12h. Molecular weights of obtained sacrificial free polymers were 28 kDa, and 17 kDa for TEM grid and gold mask, respectively. AFM images of two different surfaces show clear difference (Figure 4.4). Even though molecular weight of ITO-g-PMMA is a 1.6-fold higher for TEM grid than gold mask, film thickness (height) of ITO-g-PMMA is lower for TEM grid than gold mask. Based on equation 4.2, grafting densities of each brushes were calculated in table 4.1. We could clearly found that ITO-g-PMMA patterned with gold mask showed 2.2-fold enhanced grafting density and uniform surface than those with TEM grid, indicating that the pattering can be free from light scattering and damage of initiator from back scattering by using gold mask.

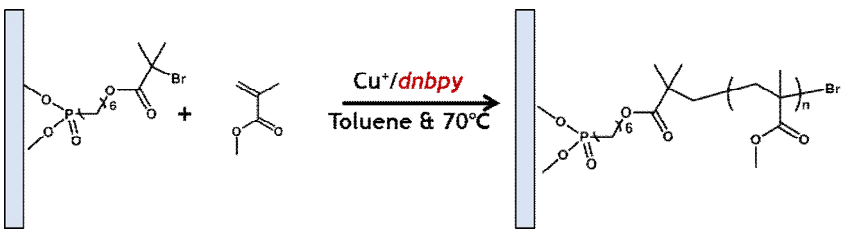


**Figure 4.3.** Schematic illustration of surface initiated ATRP of PMMA.

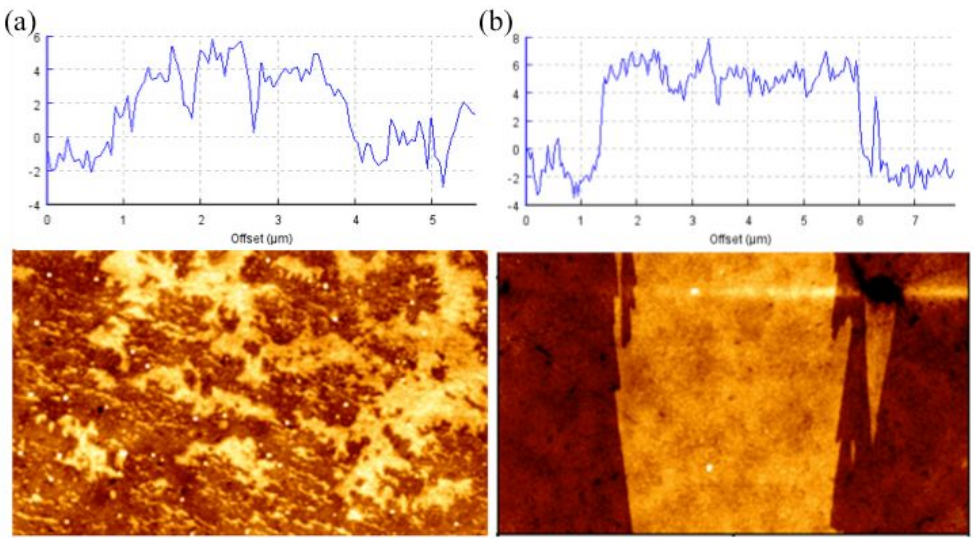


**Figure 4.4.** AFM image and height trace of ITO-g-PMMA patterned by (a) TEM grid, and (b) gold mask.

**Table 4.1.** Molecular weights, heights, and grafting densities of two different ITO-*g*-PMMA patterned by TEM grid and gold mask.

| Shadow mask | $M_n$ (g/mol) | Height (nm) | Grafting Density[⑦] (Chains/nm$^2$) |
|---|---|---|---|
| TEM grid | 28000 | 6 | 0.15 |
| Gold mask | 17000 | 8 | 0.331 |

⑦ Bulk density of PMMA (ρ) is 1.17.

### 4.3.2. Control of grafting density by varying concentration of initiator

In section 4.2, we already discussed that effect of initiator concentration on surface, initiation efficiency, and growing radical control on grafting density and features of polymer brushes. In chapter 2, kinetics of ATRP with PFPMA monomer was fully studied to enhance initiation efficiency and control of growing radical. As a result, we enabled to achieve high initiation efficiency (more than 80 % for both low molecular weight (DP=80~90 %) and high molecular weight (DP=200~220)) and narrow PDI with reasonable molecular weight with its theoretical value, indication better control of growing radical.

Effect of concentration of initiator on grafting density was studied by varying concentration of initiator solution from 0.5 mM to 10 mM in toluene. ITO substrates were immersed into different concentration of initiator solution for fabricating self-assembled monolayer on ITO surface. Those modified ITO substrates were placed in same ATRP solution to polymerized ITO-g-poly(PFPMA) under same condition (Figure 4.5). The molecular weight of resulting sacrificial polymer is 33 kDa with 1.17 of polydispersity. Surface of ITO-g-poly(PFPMA) was characterized by AFM (Figure 4.6). Through AFM height measurement, height of ITO-g-poly(PFPMA) was increased from 2 nm to 8 nm for modified ITO substrates which was immersed in initiator solution with concentration of 0.5 mM

to 5 mM, and decreased to 3 nm for that with 10 mM.

In order to calculate grafting density based on AFM height data, the bulk density of poly(PFPMA) (ρ) was needed to calculate. The bulk density of poly(PFPMA) was calculated based on relationship between molar mass and molar volume on bulk density of polymer ($\rho = M_r/V_r$, where $M_r$ is molar mass and $V_r$ is molar volume). Molar volume ($V_r$) of poly(PFPMA), however, still remained as a unknown value. This was calculated based on relation between $V_r$ and $V_w$ ($V_r=V_w \times 1.60 \pm 0.045$ for glassy amorphous polymers) and group increment of $V_w$ reported by van Krevelen, D. W.,[176] where $V_r$ is molar volume of polymer calculated from density, $V_w$ is Van der Waals volume (Table 4.2).

Based on calculated bulk density (ρ) of poly(PFPMA), grafting density of ITO-g-poly(PFPMA) was calculated (Table 4.3) and clearly showed dependence on concentration of initiator. Since the grafting density is proportional to height ($\sigma =(h\rho N_A)/M_n$) for same polymer with same molecular weight, grafting density showed similar behavior with change of height, indicating grafting density was highly affected by concentration of initiator on ITO surface. Decreasing of grafting density with ITO modified with 10 mM was noticeable. This tendency might be caused by termination between neighboring initiator as distance between them decreased.[170] Thus, concentration of initiator is important as radical control to prepare polymer brushes with high grafting density. Furthermore, grafting density with higher value (0.2 chains/nm$^2$) is comparable with previously reported value (0.2 chains/nm$^2$) of poly(PFPA) prepared by surface initiated RAFT.[167]

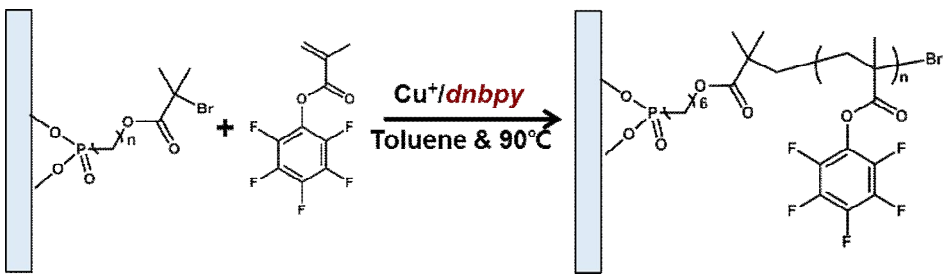


**Figure 4.5.** Schematic illustration of surface initiated ATRP of PFPMA.

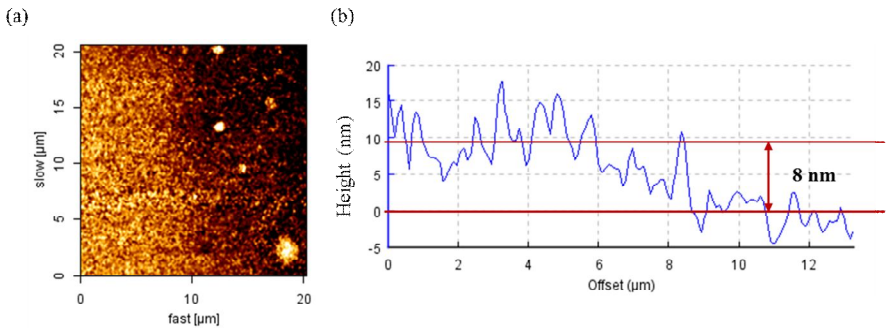


**Figure 4.6** Surface characterization of (a) AFM image, and (b) AFM height trace for ITO-g-PFPMA.

**Table 4.2.** Calculation of polymeric density of PFPMA.

| Group increments | | $V_{wi}$ |
|---|---|---|
| 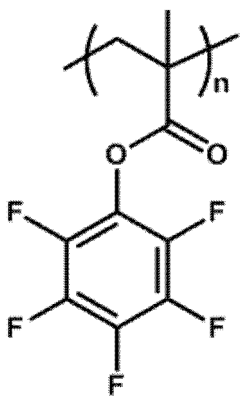 | -CH2- | 10.23 |
| | >C< (tetra-) | 3.3 |
| | -CH3 | 13.67 |
| | -COO- | 15.2 |
| | -phenyl (hexa-) | 33.3 |
| | -F (×5) | 5.7 (×5) |
| Total Van der Waals Volume ($V_{wi}$) | | 104.2 |
| Total molar Volume ($V_i$=1.6 × $V_{wi}$) | | 166.72 |
| Molar mass of repreat unit (g/mol) | | 252.14 |
| Density of repreat unit (g/cm3) | | **1.51** |

**Table 4.3.** Relationship between concentration of initiator solution and grafting density

| Concentration | $M_n$ (g/mol) | Height (nm) | Grafting Density (Chains/nm$^2$) |
|---|---|---|---|
| 0.5mM | 33000 | 2 | 0.06 |
| 1mM | 33000 | 4 | 0.11 |
| 5mM | 33000 | 8 | 0.22 |
| 10mM | 33000 | 3 | 0.08 |

### 4.3.3 Post polymerization modification of polymer brushes

The possibility of modular synthesis of functional polymer brushes from reactive polymer brush platforms was tested by post polymerization modification of ITO-*g*-poly(PFPMA) with amine containing functional molecules. 4-amino-2,2,6,6,-tetramethylpiperidine 1-oxyl (4-amino-TEMPO) which are known for reversible redox electrochemical property with long term stability was chosen as a model molecule for investigating the possibility on preparation of surface with electrochemical properties. The ITO-*g*-poly(PFPMA) was immersed in 5 M (1 wt%) of 4-(amino-TEMPO) solution in THF for 48 h in pre-heated oil bath at 50 °C (Figure 4.7). The 4-(amino-TEMPO) treated ITO-g-poly(PFPMA) (ITO-g-poly(TEMPO)) was rinsed several times and sonicated in THF, Toluene, and Ethanol for 15 min, respectively, to remove residual 4-(amino-TEMPO). In order to characterize surface properties of polymer brushes, several characterization techniques such as FT-IR, contact Angle, and X-ray photoelectron spectroscopy (XPS) were conducted.

FT-IR spectra of ITO-g-poly(PFPMA) and 4-(amino-TEMPO) treated ITO-g-poly(PFPMA) (ITO-g- poly(TEMPO)) indicated that 4-(amino-TEMPO) was successfully substituted into poly(PFPMA) chain without hydrolysis of PFP group based on formation of amide peak at 1650 $cm^{-1}$ and reduction and ester peak at 1780 $cm^{-1}$, also absence of O-H stretch band around 3500 $cm^{-1}$ (Figure 4.8). Contact Angle also supported qualitative substitution based on the change of

surface properties. Contact angle of surface was increased from 92 $^{o}$ to 106$^{o}$ after polymerization of poly(PFPMA) brushes due to increase of hydrophobic PFP groups, and those was decreased to 82 $^{o}$ after 4-(amino-TEMPO) substitution due to decrease of PFP groups.

In order to characterize quantitative amount of substitution, XPS measurement was conducted. XPS spectrum of ITO-*g*-poly(PFPMA) has big F1s peak at 688 eV, while that of ITO-*g*-poly(TEMPO) did not. While the change after substitution in C1s range is tricky to distinguish since C-F (at 288 eV), C-O (286 eV), C=O (287 eV), changing of ester to amide bond is all at 289 eV,[177-179] C-C bond at 285 eV was clearly decreased. Furthermore, F ls at 688 eV is negative for ITO-*g*-poly(TEMPO) after substitution, indicating 100% of conversion (Figure 4.9).

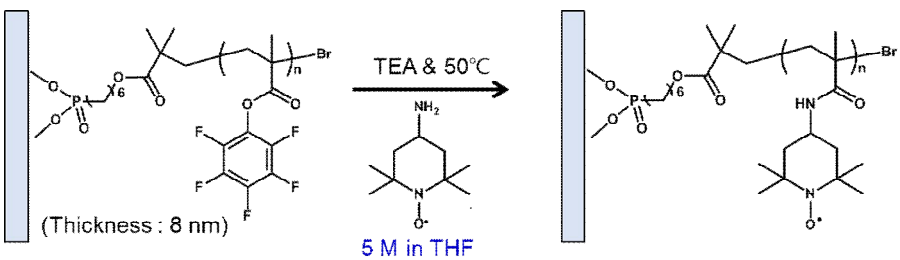


**Figure 4.7.** Schematic illustration of post-modification of ITO-g-PFPMA by treating with 4-(amino-TEMPO).

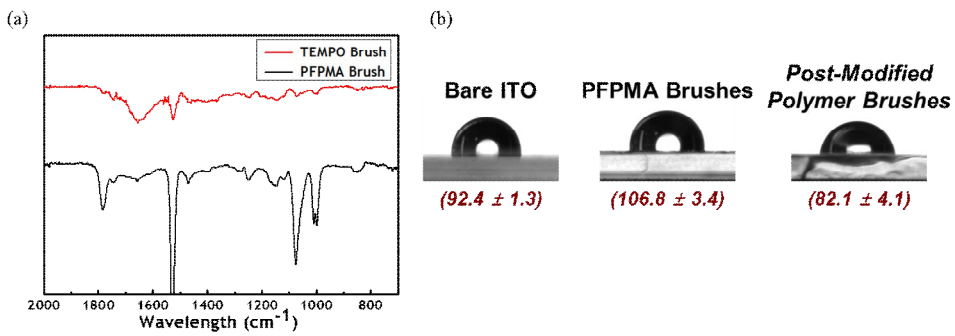


**Figure 4.8.** (a) FT-IR spectrum and (b) contact angle change of ITO-g-p(PFPMA_ and ITO-g-p(TEMPO).

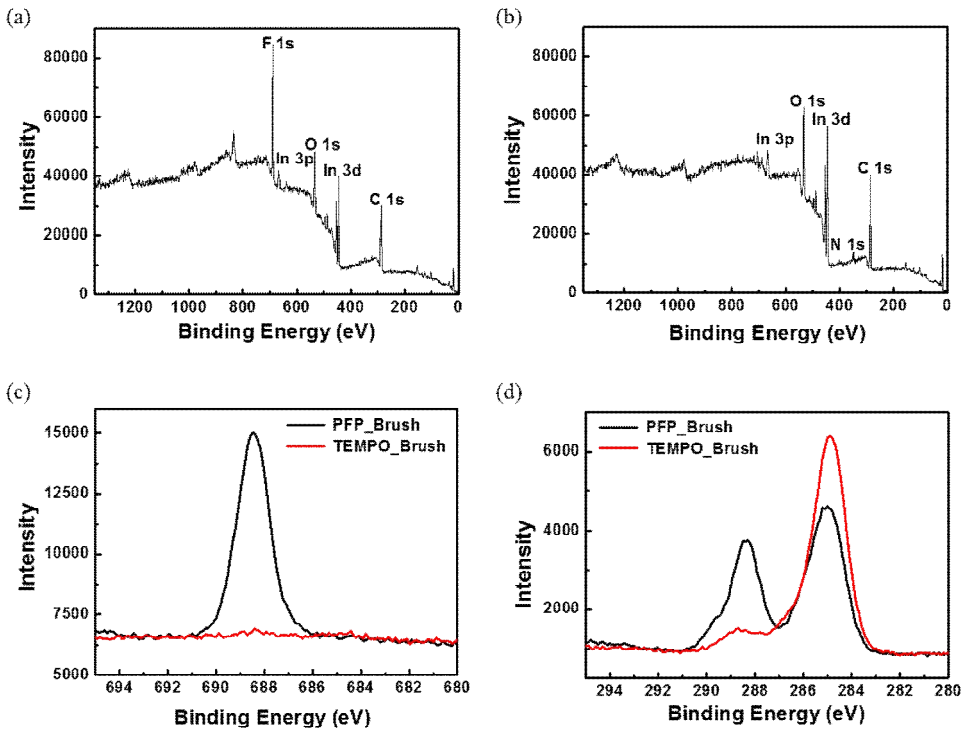


**Figure 4.9.** XPS spectra of (a) ITO-*g*-p(PFPMA), (b) ITO-*g*-p(TEMPO), and comparisons of XPS spectra of ITO-*g*-p(PFPMA) and ITO-*g*-p(TEMPO) at (c) F 1s and (d) C ls.

## 4.4 Conclusion

The reactive polymer brushes platform was demonstrated by surface initiated ATRP of PFPMA monomers under optimized ATRP condition for high molecular weight of poly(PFPMA) in solution. Proper pattering technique and concentration of initiator was optimized by changing patterning mask and concentration of initiator. By comparing PMMA brushes growing from patterned surface by selective deactivation of initiator with TEM mask or gold shadow mask, gold shadow mask show better selectivity with clear patterning and higher grafting density. Furthermore, when concentration of initiator solution was 5 mM in toluene, the height (8 nm) and grafting density (0.2 chains/$nm^2$) was highest value compared with others. We could prove that our polymer brushes platform enable to convert their properties by post polymerization modification through 100 % of replacement without side reaction of 4-(amino-TEMPO). We believe that out platform will open new strategy to prepare functional polymer brushes without difficult synthesis and modification step to applied electrical application.

# Chapter 5. Conclusion and Outlook

Ceaseless efforts on optimizing condition for ATRP of PFPMA open new strategy for preparing versatile reactive polymers and reactive polymer platforms. This thesis was started with challenge on ATRP of PFPMA to mutual complementation of their shortcomings. ATRP of PFPMA will widen application fields of their polymer which cannot covered with other control radical polymerization (ROMP, RAFT, and NMP) and be accessibility because of commercial components for ATRP. While kinetics of ATRP with PFPMA is still not ideal, an in-depth study on ATRP of PFPMA was first and achieved well-defined polymer with narrow polydispersity (<1.2) and highest molecular weight more than 60 kDa, which is not possible in previous researches.

The nanoprecipitation method allows fast and simple preparation of particles with size tunability and surfactant-free surface. Furthermore, photo-reversible dimerization allows structural stability of polymer nanoparticles, resulting robust reactive polymer nanoparticle platforms, which is stable under good solvent for parent polymer and high temperature up to 70 °C. Three different fluorescent polymer nanoparticles, which emit blue, green, red fluorescent by imparting coumarin, dansylcadaverine, and spiropyran, were demonstrated from those reactive nanoparticle platform, indicating facile control of emission wavelength without difficult design and control of bandgap to realize fluorescent

polymer nanoparticles. Furthermore, thermos-responsive polymer nanoparticles and photo-responsive polymer nanoparticles were prepared by treating with not only small molecules such as isopropylamine and spiropyran but also amine terminated polymer like poly(NIPAAm) from same platform. By employing various functionality into those reactive platforms, we proved that our reactive polymer nanoparticle platforms were versatile with facile control of functionality from fluorescent to stimuli-responsiveness and potential for multifunctional or smart actuator for bio imaging or display.

Surface initiated ATRP is long-cherished wish to prepared reactive polymer brush platforms. Demonstration of those reactive polymer brush platforms (ITO-*g*-poly(PFPMA)) was eventually available after optimal condition of ATRP with PFPMA in solution was in hand. In order to achieve enough coverage, high molecular weight of poly(PFPMA) and grafting density were required. By varying the concentration of initiator solution in toluene for modification of ITO substrates, we could controlled grafting density from 0.06 to 0.2 chains/nm$^2$ which are mushroom regime to polymer brushes regime. Furthermore, we evaluate the possibility of modification by treating the ITO-*g*-poly(TEMPO) with 4-(amino-TEMPO). FT-IR spectra, contact angle measurement and XPS spectra confirmed that substitution was occurs successfully with high yield (99%). These results means that facile preparation of electro-active surface from ITO was possible by simple post polymerization modification and enabled to apply in biosensor, smart windows, organic batteries, or organic memory devices.

We believed that our strategy will widen application fields of polymer matrices by allowing facile preparation of function polymer with desired properties and structure for particular applications.

# Bibliography

[1] G. Inzelt, M. Pineri, J. W. Schultze and M. A. Vorotyntsev, *Electrochimica Acta* **2000**, *45*, 2403-2421.

[2] H. Shirakawa, E. J. Louis, A. G. MacDiarmid, C. K. Chiang and A. J. Heeger, *Journal of the Chemical Society, Chemical Communications* **1977**, 578-580.

[3] R. H. Friend, R. W. Gymer, A. B. Holmes, J. H. Burroughes, R. N. Marks, C. Taliani, D. D. C. Bradley, D. A. D. Santos, J. L. Bredas, M. Logdlund and W. R. Salaneck, *Nature* **1999**, *397*, 121-128.

[4] N. C. Greenham, X. Peng and A. P. Alivisatos, *Physical Review B* **1996**, *54*, 17628-17637.

[5] J. Song, J. Lim, D. Lee, M. Thambidurai, J. Y. Kim, M. Park, H.-J. Song, S. Lee, K. Char and C. Lee, *ACS Applied Materials & Interfaces* **2015**, *7*, 18460-18466.

[6] W. T. Choi, J. Song, J. Ko, Y. Jang, T.-H. Kim, Y.-S. Han, J. Lim, C. Lee and K. Char, *Journal of Polymer Science Part B: Polymer Physics* **2016**, *54,* 128-134.

[7] T. Kim, H. Yoon, H.-J. Song, N. Haberkorn, Y. Cho, S. H. Sung, C. H. Lee, K. Char and P. Theato, *Macromolecular Rapid Communications* **2012**, *33*, 2035-2040.

[8] Y.-J. Cheng, S.-H. Yang and C.-S. Hsu, *Chemical Reviews* **2009**, *109*, 5868-5923.

[9] T. D. Nguyen, G. Hukic-Markosian, F. Wang, L. Wojcik, X.-G. Li, E. Ehrenfreund and Z. V. Vardeny, *Nat Mater* **2010**, *9*, 345-352.

[10] T. Piok, S. Gamerith, C. Gadermaier, H. Plank, F. P. Wenzl, S. Patil, R. Montenegro, T. Kietzke, D. Neher, U. Scherf, K. Landfester and E. J. W. List, *Advanced Materials* **2003**, *15*, 800-804.

[11] E. Mecher, F. Gallego-Gomez, H. Tillmann, H.-H. Horhold, J. C. Hummelen and K. Meerholz, *Nature* **2002**, *418*, 959-964.

[12] B. Kippelen, S. R. Marder, E. Hendrickx, J. L. Maldonado, G. Guillemet, B. L. Volodin, D. D. Steele, Y. Enami, Sandalphon, Y. J. Yao, J. F. Wang, H. Röckel, L. Erskine and N. Peyghambarian, *Science* **1998**, *279*, 54-57.

[13] C. Fan, K. W. Plaxco and A. J. Heeger, *Journal of the American Chemical Society* **2002**, *124*, 5642-5643.

[14] A. Rose, Z. Zhu, C. F. Madigan, T. M. Swager and V. Bulovic, *Nature* **2005**, *434*, 876-879.

[15] M. A. C. Stuart, W. T. S. Huck, J. Genzer, M. Muller, C. Ober, M. Stamm, G. B. Sukhorukov, I. Szleifer, V. V. Tsukruk, M. Urban, F. Winnik, S. Zauscher, I. Luzinov and S. Minko, *Nat Mater* **2010**, *9*, 101-113.

[16] D. Schmaljohann, *Advanced Drug Delivery Reviews* **2006**, *58*, 1655-1670.

[17] I. Berndt and W. Richtering, *Macromolecules* **2003**, *36*, 8780-8785.

[18] R. Byrne, C. Ventura, F. Benito Lopez, A. Walther, A. Heise and D. Diamond, *Biosensors and Bioelectronics* **2010**, *26*, 1392-1398.

[19] D. Kessler, F. D. Jochum, J. Choi, K. Char and P. Theato, *ACS Applied Materials & Interfaces* **2011**, *3*, 124-128.

[20] W. Zhang and H. Choi, *Polymers* **2014**, *6*, 2803.

[21] F. D. Jochum, P. J. Roth, D. Kessler and P. Theato, *Biomacromolecules* **2010**, *11*, 2432-2439.

[22] J. L. Zhang, R. S. Srivastava and R. D. K. Misra, *Langmuir* **2007**, *23*, 6342-6351.

[23] J.-H. Lee, H. J. Hwang, G. Bhak, Y. Jang, S. R. Paik and K. Char, *ACS Macro Letters* **2013**, *2*, 688-693.

[24] L. Ruiz-Pérez, A. Pryke, M. Sommer, G. Battaglia, I. Soutar, L. Swanson and M. Geoghegan, *Macromolecules* **2008**, *41*, 2203-2211.

[25] Y. Cho, J. Lim and K. Char, *Soft Matter* **2012**, *8*, 10271-10278.

[26] M. A. Nash and H. E. Gaub, *ACS Nano* **2012**, *6*, 10735-10742.

[27] S. H. Anastasiadis, M. I. Lygeraki, A. Athanassiou, M. Farsari and D. Pisignano, *Journal of Adhesion Science and Technology* **2008**, *22*, 1853-1868.

[28] Q. Zhang, N. Re Ko and J. Kwon Oh, *Chemical Communications* **2012**, *48*, 7542-7552.

[29] M. Zrínyi, A. Szilágyi, G. Filipcsei, J. Fehér, J. Szalma and G. Móczár, *Polymers for Advanced Technologies* **2001**, *12*, 501-505.

[30] H. Lee, S. M. Dellatore, W. M. Miller and P. B. Messersmith, *Science* **2007**, *318*, 426-430.

[31] D. Wenzlik, C. Ohm, C. Serra and R. Zentel, *Soft Matter* **2011**, *7*, 2340-2344.

[32] H. Yoon, A. Ghosh, J. Y. Han, S. H. Sung, W. B. Lee and K. Char, *Advanced Functional Materials* **2012**, *22*, 3723-3728.

[33] J. Hong, W. K. Bae, H. Lee, S. Oh, K. Char, F. Caruso and J. Cho, *Advanced*

*Materials* **2007**, *19*, 4364-4369.

[34] G. R. Whittell and I. Manners, *Advanced Materials* **2007**, *19*, 3439-3468.

[35] G. R. Whittell, M. D. Hager, U. S. Schubert and I. Manners, *Nat Mater* **2011**, *10*, 176-188.

[36] G. W. M. Vandermeulen, K. T. Kim, Z. Wang and I. Manners, *Biomacromolecules* **2006**, *7*, 1005-1010.

[37] B.-Y. Kim, E. L. Ratcliff, N. R. Armstrong, T. Kowalewski and J. Pyun, *Langmuir* **2010**, *26*, 2083-2092.

[38] A. Breivogel, M. Park, D. Lee, S. Klassen, A. Kühnle, C. Lee, K. Char and K. Heinze, *European Journal of Inorganic Chemistry* **2014**, *2014*, 288-295.

[39] A. Breivogel, S. Wooh, J. Dietrich, T. Y. Kim, Y. S. Kang, K. Char and K. Heinze, *European Journal of Inorganic Chemistry* **2014**, *2014*, 2720-2734.

[40] Z. Zhang, W. Feng, P. Su, X. Lü, J. Song, D. Fan, W.-K. Wong, R. A. Jones and C. Su, *Inorganic Chemistry* **2014**, *53*, 5950-5960.

[41] J. Zou, F. Zhang, S. Zhang, S. F. Pollack, M. Elsabahy, J. Fan and K. L. Wooley, *Advanced Healthcare Materials* **2014**, *3*, 441-448.

[42] A. A. Golriz, T. Kaule, J. Heller, M. B. Untch, P. Schattling, P. Theato, M. Toda, S. Yoshida, T. Ono, H.-J. Butt, J. S. Gutmann and R. Berger, *Nanoscale* **2011**, *3*, 5049-5058.

[43] S. C. Thickett and R. G. Gilbert, *Polymer* **2007**, *48*, 6965-6991.

[44] R. K. Iha, K. L. Wooley, A. M. Nyström, D. J. Burke, M. J. Kade and C. J. Hawker, *Chemical Reviews* **2009**, *109*, 5620-5686.

[45] C. E. Hoyle and C. N. Bowman, *Angewandte Chemie International Edition* **2010**, *49*, 1540-1573.

[46] A. Sanyal, *Macromolecular Chemistry and Physics* **2010**, *211*, 1417-1425.

[47] B. D. Mather, K. Viswanathan, K. M. Miller and T. E. Long, *Progress in Polymer Science* **2006**, *31*, 487-531.

[48] A. J. C. Kuehne, M. C. Gather and J. Sprakel, *Nat Commun* **2012**, *3*, 1088.

[49] C. K. F. M. A. F. S. Alexandridou, *Journal of Microencapsulation* **2001**, *18*, 767-781.

[50] J. K. Oh, F. Perineau and K. Matyjaszewski, *Macromolecules* **2006**, *39*, 8003-8010.

[51] R. Gurny, N. A. Peppas, D. D. Harrington and G. S. Banker, *Drug Development and Industrial Pharmacy* **1981**, *7*, 1-25.

[52] C. Wu, C. Szymanski and J. McNeill, *Langmuir* **2006**, *22*, 2956-2960.

[53] K. Kataoka, A. Harada and Y. Nagasaki, *Advanced Drug Delivery Reviews* **2001**, *47*, 113-131.

[54] Y.-P. Sun and H. W. Rollins, *Chemical Physics Letters* **1998**, *288*, 585-588.

[55] J. Seo, J. L. Lutkenhaus, J. Kim, P. T. Hammond and K. Char, *Langmuir* **2008**, *24*, 7995-8000.

[56] H. S. Suh, H. Kang, P. F. Nealey and K. Char, *Macromolecules* **2010**, *43*, 4744-4751.

[57] J. Huang, H. Murata, R. R. Koepsel, A. J. Russell and K. Matyjaszewski, *Biomacromolecules* **2007**, *8*, 1396-1399.

[58] D. M. Jones, J. R. Smith, W. T. S. Huck and C. Alexander, *Advanced Materials* **2002**, *14*, 1130-1134.

[59] H.-U. Blaser, C. Malan, B. Pugin, F. Spindler, H. Steiner and M. Studer, *Advanced Synthesis & Catalysis* **2003**, *345*, 103-151.

[60] S. R. Neufeldt and M. S. Sanford, *Accounts of Chemical Research* **2012**, *45*, 936-946.

[61] L. R. Domingo, E. Chamorro and P. Pérez, *The Journal of Organic Chemistry* **2008**, *73*, 4615-4624.

[62] H. G. Batz, G. Franzmann and H. Ringsdorf, *Die Makromolekulare Chemie* **1973**, *172*, 27-47.

[63] P. Ferruti, A. Bettelli and A. Feré, *Polymer* **1972**, *13*, 462-464.

[64] P. Theato, *Journal of Polymer Science Part A: Polymer Chemistry* **2008**, *46*, 6677-6687.

[65] M. Eberhardt, R. Mruk, R. Zentel and P. Théato, *European Polymer Journal* **2005**, *41*, 1569-1575.

[66] J.-C. Blazejewski, J. W. Hofstraat, C. Lequesne, C. Wakselman and U. E. Wiersum, *Journal of Fluorine Chemistry* **1999**, *97*, 191-199.

[67] N. Vogel and P. Théato, *Macromolecular Symposia* **2007**, *249-250*, 383-391.

[68] M. Eberhardt and P. Théato, *Macromolecular Rapid Communications* **2005**, *26*, 1488-1493.

[69] N. Metz and P. Theato, *European Polymer Journal* **2007**, *43*, 1202-1209.

[70] K. Matyjaszewski and J. Xia, *Chem. Rev. (Washington, DC, U. S.)* **2001**, *101*,

2921.

[71] K. Matyjaszewski, D. A. Shipp, J.-L. Wang, T. Grimaud and T. E. Patten, *Macromolecules* **1998**, *31*, 6836-6840.

[72] W. Tang, Y. Kwak, W. Braunecker, N. V. Tsarevsky, M. L. Coote and K. Matyjaszewski, *Journal of the American Chemical Society* **2008**, *130*, 10702-10713.

[73] A. J. D. Magenau, Y. Kwak, K. Schröder and K. Matyjaszewski, *ACS Macro Letters* **2012**, *1*, 508-512.

[74] H. Zhao, W. Gu, M. W. Thielke, E. Sterner, T. Tsai, T. P. Russell, E. B. Coughlin and P. Theato, *Macromolecules* **2013**, *46*, 5195-5201.

[75] X. S. Li, L. H. Gan and Y. Y. Gan, *Polymer* **2008**, *49*, 1879-1884.

[76] N. K. Singha, M. I. Gibson, B. P. Koiry, M. Danial and H.-A. Klok, *Biomacromolecules* **2011**, *12*, 2908-2913.

[77] F. Lince, D. L. Marchisio and A. A. Barresi, *Journal of Colloid and Interface Science* **2008**, *322*, 505-515.

[78] K. Matyjaszewski, P. J. Miller, N. Shukla, B. Immaraporn, A. Gelman, B. B. Luokala, T. M. Siclovan, G. Kickelbick, T. Vallant, H. Hoffmann and T. Pakula, *Macromolecules* **1999**, *32*, 8716-8724.

[79] F. D. Jochum and P. Theato, *Macromolecules* **2009**, *42*, 5941-5945.

[80] Y. Lee, S. Hanif, P. Theato, R. Zentel, J. Lim and K. Char, *Macromolecular Rapid Communications* **2015**, *36*, 1089-1095.

[81] H. Fischer, *Journal of Polymer Science Part A: Polymer Chemistry* **1999**, *37*,

1885-1901.

[82] O. Lunov, T. Syrovets, C. Loos, J. Beil, M. Delacher, K. Tron, G. U. Nienhaus, A. Musyanovych, V. Mailänder, K. Landfester and T. Simmet, *ACS Nano* **2011**, *5*, 1657-1669.

[83] B. V. Parakhonskiy, A. M. Yashchenok, M. Konrad and A. G. Skirtach, *Advances in Colloid and Interface Science* **2014**, *207*, 253-264.

[84] O. Lehmann, H. Meyssamy, K. Kömpe, H. Schnablegger and M. Haase, *The Journal of Physical Chemistry B* **2003**, *107*, 7449-7453.

[85] D. Radziuk, A. Skirtach, A. Geßner, M. U. Kumke, W. Zhang, H. Möhwald and D. Shchukin, *Langmuir* **2011**, *27*, 14472-14480.

[86] P. Alivisatos, *Nat Biotechnol* **2004**, *22*, 47-52.

[87] J. K. Jaiswal, H. Mattoussi, J. M. Mauro and S. M. Simon, *Nat Biotech* **2003**, *21*, 47-51.

[88] X. Michalet, F. F. Pinaud, L. A. Bentolila, J. M. Tsay, S. Doose, J. J. Li, G. Sundaresan, A. M. Wu, S. S. Gambhir and S. Weiss, *Science* **2005**, *307*, 538-544.

[89] H. Ow, D. R. Larson, M. Srivastava, B. A. Baird, W. W. Webb and U. Wiesner, *Nano Letters* **2004**, *5*, 113-117.

[90] S. C. Warren, F. J. DiSalvo and U. Wiesner, *Nat Mater* **2007**, *6*, 156-161.

[91] C. Szymanski, C. Wu, J. Hooper, M. A. Salazar, A. Perdomo, A. Dukes and J. McNeill, *The Journal of Physical Chemistry B* **2005**, *109*, 8543-8546.

[92] C. Cordovilla and T. M. Swager, *Journal of the American Chemical Society* **2012**, *134*, 6932-6935.

[93] S. Sharifi, S. Behzadi, S. Laurent, M. Laird Forrest, P. Stroeve and M. Mahmoudi, *Chemical Society Reviews* **2012**, *41*, 2323-2343.

[94] O. I. Micic, C. J. Curtis, K. M. Jones, J. R. Sprague and A. J. Nozik, *The Journal of Physical Chemistry* **1994**, *98*, 4966-4969.

[95] J. Lim, W. K. Bae, D. Lee, M. K. Nam, J. Jung, C. Lee, K. Char and S. Lee, *Chemistry of Materials* **2011**, *23*, 4459-4463.

[96] S. J. Soenen, B. B. Manshian, T. Aubert, U. Himmelreich, J. Demeester, S. C. De Smedt, Z. Hens and K. Braeckmans, *Chemical Research in Toxicology* **2014**, *27*, 1050-1059.

[97] J. W. Vanderhoff, M. S. El-Aasser and J. Ugelstad in *Polymer emulsification process*, *Vol.* Google Patents, **1979**.

[98] J. Lim and T. M. Swager, *Angewandte Chemie International Edition* **2010**, *49*, 7486-7488.

[99] H. Fessi, F. Puisieux, J. P. Devissaguet, N. Ammoury and S. Benita, *International Journal of Pharmaceutics* **1989**, *55*, R1-R4.

[100] K. Landfester, *Advanced Materials* **2001**, *13*, 765-768.

[101] F. Gaudin and N. Sintes-Zydowicz, *Colloids and Surfaces A: Physicochemical and Engineering Aspects* **2008**, *331*, 133-142.

[102] J. P. Rao and K. E. Geckeler, *Progress in Polymer Science* **2011**, *36*, 887-913.

[103] M. Elsabahy, S. Zhang, F. Zhang, Z. J. Deng, Y. H. Lim, H. Wang, P. Parsamian, P. T. Hammond and K. L. Wooley, *Sci. Rep.* **2013**, *3*.

[104] T. Erdem, V. Ibrahimova, D.-W. Jeon, I.-H. Lee, D. Tuncel and H. V. Demir,

*The Journal of Physical Chemistry C* **2013**, *117*, 18613-18619.

[105] K. Li and B. Liu, *Journal of Materials Chemistry* **2012**, *22*, 1257-1264.

[106] L. Nuhn, M. Hirsch, B. Krieg, K. Koynov, K. Fischer, M. Schmidt, M. Helm and R. Zentel, *ACS Nano* **2012**, *6*, 2198-2214.

[107] L. Nuhn, S. Gietzen, K. Mohr, K. Fischer, K. Toh, K. Miyata, Y. Matsumoto, K. Kataoka, M. Schmidt and R. Zentel, *Biomacromolecules* **2014**, *15*, 1526-1533.

[108] W. H. Melhuish, *The Journal of Physical Chemistry* **1961**, *65*, 229-235.

[109] V. Janout, M. Lanier and S. L. Regen, *Journal of the American Chemical Society* **1997**, *119*, 640-647.

[110] V. Ferranti, H. Marchais, C. Chabenat, A. M. Orecchioni and O. Lafont, *International Journal of Pharmaceutics* **1999**, *193*, 107-111.

[111] I. Limayem Blouza, C. Charcosset, S. Sfar and H. Fessi, *International Journal of Pharmaceutics* **2006**, *325*, 124-131.

[112] L. Feng, C. Zhu, H. Yuan, L. Liu, F. Lv and S. Wang, *Chemical Society Reviews* **2013**, *42*, 6620-6633.

[113] J. Pecher and S. Mecking, *Macromolecules* **2007**, *40*, 7733-7735.

[114] J. Nicolas, S. Mura, D. Brambilla, N. Mackiewicz and P. Couvreur, *Chemical Society Reviews* **2013**, *42*, 1147-1235.

[115] J. D. Debord and L. A. Lyon, *The Journal of Physical Chemistry B* **2000**, *104*, 6327-6331.

[116] T. Kietzke, D. Neher, K. Landfester, R. Montenegro, R. Guntner and U. Scherf, *Nat Mater* **2003**, *2*, 408-412.

[117] A. Ott, X. Yu, R. Hartmann, J. Rejman, A. Schütz, M. Ochs, W. J. Parak and S. Carregal-Romero, *Chemistry of Materials* **2015**, *27*, 1929-1942.

[118] P. Schattling, F. D. Jochum and P. Theato, *Polymer Chemistry* **2014**, *5*, 25-36.

[119] L. Nuhn, M. Barz and R. Zentel, *Macromolecular Bioscience* **2014**, *14*, 607-618.

[120] J. Zhuang, S. Jiwpanich, V. D. Deepak and S. Thayumanavan, *ACS Macro Letters* **2012**, *1*, 175-179.

[121] H. Wang, J. Zhuang and S. Thayumanavan, *ACS Macro Letters* **2013**, *2*, 948-951.

[122] E. Fröhlich, *International Journal of Nanomedicine* **2012**, *7*, 5577-5591.

[123] M. K. Yu, J. Park and S. Jon, *Theranostics* **2012**, *2*, 3-44.

[124] P. Schattling, F. D. Jochum and P. Theato, *Chemical Communications* **2011**, *47*, 8859-8861.

[125] S. Mavila, O. Eivgi, I. Berkovich and N. G. Lemcoff, *Chemical Reviews* **2015,** ASAP (DOI: 10.1021/acs.chemrev.5b00290).

[126] R. J. Wojtecki, M. A. Meador and S. J. Rowan, *Nat Mater* **2011**, *10*, 14-27.

[127] P. T. Dirlam, H. J. Kim, K. J. Arrington, W. J. Chung, R. Sahoo, L. J. Hill, P. J. Costanzo, P. Theato, K. Char and J. Pyun, *Polymer Chemistry* **2013**, *4*, 3765-3773.

[128] E. H. H. Wong, S. J. Lam, E. Nam and G. G. Qiao, *ACS Macro Letters* **2014**, *3*, 524-528.

[129] G. Kaur, P. Johnston and K. Saito, *Polymer Chemistry* **2014**, *5*, 2171-2186.

[130] W. Fan, X. Tong, Q. Yan, S. Fu and Y. Zhao, *Chemical Communications* **2014**, *50*, 13492-13494.

[131] X. Zhang, Y. Gao, Y. Lin, J. Hu and Y. Ju, *Polymer Chemistry* **2015**, *6*, 4162-4166.

[132] Z. Yu, J. Zhang, R. J. Coulston, R. M. Parker, F. Biedermann, X. Liu, O. A. Scherman and C. Abell, *Chemical Science* **2015**, *6*, 4929-4933.

[133] P. Froimowicz, H. Frey and K. Landfester, *Macromolecular Rapid Communications* **2011**, *32*, 468-473.

[134] R. Tangirala, E. Baer, A. Hiltner and C. Weder, *Advanced Functional Materials* **2004**, *14*, 595-604.

[135] J. Jiang, B. Qi, M. Lepage and Y. Zhao, *Macromolecules* **2007**, *40*, 790-792.

[136] N. Ishikawa, M. Furutani and K. Arimitsu, *ACS Macro Letters* **2015**, *4*, 741-744.

[137] S. Ghorai, J. C. Sumrak, K. M. Hutchins, D.-K. Bucar, A. V. Tivanski and L. R. MacGillivray, *Chemical Science* **2013**, *4*, 4304-4308.

[138] J. W. Chung, K. Lee, C. Neikirk, C. M. Nelson and R. D. Priestley, *Small* **2012**, *8*, 1693-1700.

[139] F. Jia, Y. Wang, H. Wang, Q. Jin, T. Cai, Y. Chen and J. Ji, *Polymer Chemistry* **2015**, *6*, 2069-2075.

[140] Y. Lee, J. Pyun, J. Lim, K. Char, Journal of Polymer Science Part A: Polymer Chemistry, accepted.

[141] A. Balbi, E. Sottofattori, T. Grandi, M. Mazzei, D. S. Pyshnyi, S. G. Lokhov

and A. V. Lebedev, *Bioorganic & Medicinal Chemistry* **1997**, *5*, 1903-1910.

[142] A. Vacca, C. Nativi, M. Cacciarini, R. Pergoli and S. Roelens, *Journal of the American Chemical Society* **2004**, *126*, 16456-16465.

[143] E. J. Foster, E. B. Berda and E. W. Meijer, *Journal of Polymer Science Part A: Polymer Chemistry* **2011**, *49*, 118-126.

[144] T. Wolff and H. Gorner, *Physical Chemistry Chemical Physics* **2004**, *6*, 368-376.

[145] B. S. Lukyanov and M. B. Lukyanova, *Chemistry of Heterocyclic Compounds* **2005**, *41*, 281-311.

[146] H. G. Schild, *Progress in Polymer Science* **1992**, *17*, 163-249.

[147] M. I. Gibson and R. K. O'Reilly, *Chemical Society Reviews* **2013**, *42*, 7204-7213.

[148] S. T. Milner, *Science (Washington, D. C., 1883-)* **1991**, *251*, 905-914.

[149] Y. Tsujii, K. Ohno, S. Yamamoto, A. Goto and T. Fukuda, *Adv. Polym. Sci.* **2006**, *197*, 1-45.

[150] R. Barbey, L. Lavanant, D. Paripovic, N. Schuwer, C. Sugnaux, S. Tugulu and H.-A. Klok, *Chem. Rev. (Washington, DC, U. S.)* **2009**, *109*, 5437-5527.

[151] S. Tugulu, P. Silacci, N. Stergiopulos and H.-A. Klok, *Biomaterials* **2007**, *28*, 2536-2546.

[152] S. Kumar, X. Tong, Y. L. Dory, M. Lepage and Y. Zhao, *Chemical Communications* **2013**, *49*, 90-92.

[153] Z. B. Zhang, S. J. Yuan, X. L. Zhu, K. G. Neoh and E. T. Kang, *Biosens.*

*Bioelectron.* **2010**, *25*, 1102-1108.

[154] M. Welch, A. Rastogi and C. Ober, *Soft Matter* **2011**, *7*, 297-302.

[155] F. Zhou and W. T. S. Huck, *Phys. Chem. Chem. Phys.* **2006**, *8*, 3815-3823.

[156] S. Minko, *Polym. Rev. (Philadelphia, PA, U. S.)* **2006**, *46*, 397-420.

[157] Y.-H. Wang, M.-K. Hung, C.-H. Lin, H.-C. Lin and J.-T. Lee, *Chem. Commun. (Cambridge, U. K.)* **2011**, *47*, 1249-1251.

[158] M. C. Tria, J. Y. Park and R. Advincula, *Chem. Commun. (Cambridge, U. K.)* **2011**, *47*, 2393-2395.

[159] W. J. Brittain and S. Minko, *J. Polym. Sci., Part A: Polym. Chem.* **2007**, *45*, 3505-3512.

[160] T. Wu, K. Efimenko and J. Genzer, *Journal of the American Chemical Society* **2002**, *124*, 9394-9395.

[161] T. Sakakiyama, H. Ohkita, M. Ohoka, S. Ito, Y. Tsujii and T. Fukudal, *Chemistry Letters* **2005**, *34*, 1366-1367.

[162] C. D. Grande, M. C. Tria, G. Jiang, R. Ponnapati and R. Advincula, *Macromolecules (Washington, DC, U. S.)* **2011**, *44*, 966-975.

[163] G. Jiang, R. Ponnapati, R. Pernites, M. J. Felipe and R. Advincula, *Macromolecules (Washington, DC, U. S.)* **2010**, *43*, 10262-10274.

[164] G. Ni, W. Yang, L. Bo, H. Guo, W. Zhang and J. Gao, *Chinese Science Bulletin* **2006**, *51*, 1644-1647.

[165] H. Ma, J. Hyun, P. Stiller and A. Chilkoti, *Advanced Materials* **2004**, *16*, 338-341.

[166] S. P. Cullen, X. Liu, I. C. Mandel, F. J. Himpsel and P. Gopalan, *Langmuir* **2007**, *24*, 913-920.

[167] K. A. Gunay, N. Schuwer and H.-A. Klok, *Polymer Chemistry* **2012**.

[168] J. Choi, P. Schattling, F. D. Jochum, J. Pyun, K. Char and P. Theato, *Journal of Polymer Science Part A: Polymer Chemistry* **2012**, *50*, 4010-4018.

[169] R. M. Arnold, G. R. Sheppard and J. Locklin, *Macromolecules* **2012**, *45*, 5444-5450.

[170] J. Pyun, T. Kowalewski and K. Matyjaszewski, *Macromol. Rapid Commun.* **2003**, *24*, 1043-1059.

[171] J.-B. Kim, W. Huang, M. D. Miller, G. L. Baker and M. L. Bruening, *Journal of Polymer Science Part A: Polymer Chemistry* **2003**, *41*, 386-394.

[172] W. Brittain, S. Boyes, A. Granville, M. Baum, B. Mirous, B. Akgun, B. Zhao, C. Blickle and M. Foster in *Surface Rearrangement of Diblock Copolymer Brushes—Stimuli Responsive Films*, *Vol. 198* (Ed. R. Jordan), Springer Berlin Heidelberg, **2006**, pp. 125-147.

[173] M. Husseman, E. E. Malmström, M. McNamara, M. Mate, D. Mecerreyes, D. G. Benoit, J. L. Hedrick, P. Mansky, E. Huang, T. P. Russell and C. J. Hawker, *Macromolecules* **1999**, *32*, 1424-1431.

[174] C. Donley, D. Dunphy, D. Paine, C. Carter, K. Nebesny, P. Lee, D. Alloway and N. R. Armstrong, *Langmuir* **2001**, *18*, 450-457.

[175] E. Sengupta, A. L. Domanski, S. A. L. Weber, M. B. Untch, H.-J. Butt, T. Sauermann, H. J. Egelhaaf and R. Berger, *The Journal of Physical Chemistry C*

**2011**, *115*, 19994-20001.

[176] D. W. Van Krevelen and K. Te Nijenhuis in *Chapter 4 - Volumetric Properties*, *Vol.* Eds.: D. W. V. K. by and K. T. Nijenhuis), Elsevier, Amsterdam, **2009**, pp. 71-108.

[177] L. Francesch, S. Borros, W. Knoll and R. Förch, *Langmuir* **2007**, *23*, 3927-3931.

[178] L. Duque, B. Menges, S. Borros and R. Förch, *Biomacromolecules* **2010**, *11*, 2818-2823.

[179] C. Moreno-Castilla, M. V. López-Ramón and F. Carrasco-Marín, *Carbon* **2000**, *38*, 1995-2001.

# 국문 초록

최근 생물공학, 광자학, 광전자공학 등과 같은 다양한 응용분야에서 고분자 재료의 역할이 강조되면서, 형광, 외부응답, 생체적합성과 같은 다양한 기능성 고분자 및 나노 구조 구현에 대한 연구가 큰 주목을 받아왔다. 그러나, 적용하고자 하는 분야에 따라 그 분야에서 필요로 하는 기능성과 구조를 조율해야만 하며, 요구되는 기능과 구조가 복잡할수록 더 까다롭고 복잡한 합성 및 가공 공정이 필요하게 된다. 따라서 간단한 개질을 통해 다양한 기능성 및 나노 구조 구현이 가능한 플랫폼을 개발하기 위한 연구가 중요하다.

본 박사학위 논문은 반응성 고분자인 팬타플로오로페닐 메타크릴레이트 고분자 (Poly(PFPMA))를 기반으로 반응성 나노입자 및 고분자 브러쉬 플랫폼을 구축하고자 하였다. 활성 에스터기를 갖고 있는 단량체의 경우 간단한 개질만으로 다양한 기능성 물질을 합성할 수 있다. 그 중에서도 팬타플로오로페닐 메타크릴레이트 (PFPMA)는 다양한 아민과 높은 반응성을 갖고 있으며, 하이드록시석신이미드 (*N*-hydroxysuccinimide)나 팬타플로오로페닐 아크릴레이트 (PFPA) 보다 아민과의 반응을 조율하기 좋다는 장점을 갖고 있어 널리 연구되고 있다.

1 장에서는 기능성 고분자의 정의 및 종류 합성 방법뿐만 아니라, 이러한 반응성 단량체에 대한 배경지식에 대한 문헌 조사를 진행하였다.

2장에서는, 원자전이 라디칼 중합 (ATRP)를 이용하여 Poly(PFPMA)를 합성하고, 중합반응 기작에 대한 연구로서, ATRP의 요소들과 단량체의 반응성을 고려하여 리간드 및 촉매를 선택하였다. 다양한 농도와 온도에서 반응을 진행한 결과, 팬타플로오로페닐 메타크릴레이트 (PFPMA) 단량체의 ATRP 중합조건을 확립하여 ATRP로 6만 이상의 높은 분자량 및 1.2 이하의 분자량 분포가 좁은 Poly(PFPMA) 합성을 가능하게 하였다.

3장에서는, 반응성 고분자인 Poly(PFPMA)를 플랫폼으로 하여 후개질(Post Modification)로 손쉽게 형광고분자 나노입자를 제조하는 연구를 수행하였다. 상용화된 단질카다버린 (Dansylcadaverine)을 모델염료로 선택하여 간단한 치환 및 나노침전법으로 구형의 나노입자를 제조할 수 있었으며, 합성된 나노입자는 수용액 상에서 모델염료보다 4.5배 증가된 양자효율을 보이는 것을 확인할 수 있었다. 이를 통하여, 간단한 염료의 선택으로 후개질하여 손쉽게 발광 파장을 조율할 수 있을 것으로 기대한다. 또한 빛에 감응하여 가교하는 쿠마린(Coumarin)을

도입하여 구조적으로 안정성을 갖춘 나노입자를 얻었으며, 이로 인해 추가적인 개질 및 입자 친화적인 용매 내에서도 그 입자 구조를 유지할 수 있게 하였다. 이러한 플랫폼을 단분자부터 고분자까지 다양한 기능성 물질로 개질하여 하나의 나노입자 플랫폼으로부터 다양한 외부자극 감응성(빛 및 온도) 및 발광파장을 갖는 나노입자를 간단한 후개질만으로 구현할 수 있다는 것을 증명하였다.

4장에서는, 1장에서 획득한 용액상 Poly(PFPMA)의 ATRP 중합 조건을 표면개시 ATRP에 적용하여 전도성 기판인 ITO 위에 반응성 고분자 브러쉬 플랫폼을 구현하였다. 이렇게 합성한 고분자는 0.2 chains/nm2의 그라프트 밀도(Grafting Density)를 갖고 있으며, 레독스(Redox) 특성을 갖는 4-amino-2,2,6,6,-tetramethylpiperidine 1-oxyl (4-amino TEMPO) 물질로 개질된다는 되는 것을 FT-IR, XPS, 및 접촉각 측정을 통해서 확인하였다.

이상의 연구 성과를 살펴보면, 입자 및 브러쉬 형태의 플랫폼에 기인하여 다양한 기능성을 갖는 기능성 고분자 나노구조를 손쉽게 구현할 수 있어 고분자의 응용을 보다 용이하게 하였으며, 나노이미징, 전기전자, 및 표면공학 등의 넓은 분야에 광범위하게 적용 가능할

것으로 예상된다

**주요어** : 기능성 고분자, 반응성 고분자, 원자전이 라디칼 중합법, 형광성 고분자 나노입자, 외부응답성 고분자 나노입자, 반응성 고분자 브러쉬

**학번** : 2009-23954